

GRADIENT SENSING IN EUKARYOTIC CELLS: MECHANISM AND  
SPATIOTEMPORAL DYNAMICS

By

KULANDAYAN KASI SUBRAMANIAN

A DISSERTATION PRESENTED TO THE GRADUATE SCHOOL  
OF THE UNIVERSITY OF FLORIDA IN PARTIAL FULFILLMENT  
OF THE REQUIREMENTS FOR THE DEGREE OF  
DOCTOR OF PHILOSOPHY

UNIVERSITY OF FLORIDA

2004

Copyright 2004

by

Kulandayan Kasi Subramanian

**Dedicated to my lovely family, Guru and Deivam.**

## ACKNOWLEDGMENTS

I wish to convey my sincere thanks and appreciation to my mentor, Dr. Atul Narang, for his guidance, constant encouragement and constructive criticism. I would like to thank my co-advisor, Dr. Gerry Shaw for his patient guidance and encouragement. I would also like to thank the members of my committee, Dr. Ranga Narayanan, Dr. Lewis Johns, Dr. Rich Dickinson and Dr. Daniel Purich, for their advice and availability. I take this opportunity to thank Dr. Orion Weiner, Harvard, for his support with the HL60 cell line. I also wish to thank Dr. Sergei Pilyugin for his advice regarding the model analysis.

I would like to thank my group members, Shakti, Eric, Ved, Jason, Greg, Ashely, Brent and other graduate students in the department for their support and friendship. I am very grateful to the members of the Shaw lab, Cui and Silas, for their help and laboratory assistance. I owe many thanks to Saurabh, Lyle and Field for their help during the course of the work. I am grateful to Tim Vaught, Microscopy Core Facility, for help with microscopy. Special thanks go to Sriks, KK, Thamba, Hari, Omar, Jeff, Maddy, Subby, Vijay, Subbu, Bullet and all my other friends for their constant support and help.

Finally, I want to express my deep gratitude and love for my parents, brothers and other family members for their unwavering support and encouragement.

## TABLE OF CONTENTS

	<u>Page</u>
ACKNOWLEDGMENTS .....	iv
LIST OF TABLES .....	viii
LIST OF FIGURES .....	ix
ABSTRACT .....	xi
 CHAPTER	
1 GRADIENT SENSING IN EUKARYOTIC CELLS .....	1
Introduction .....	1
Identification of the First Polarized Component .....	4
Spatiotemporal Dynamics .....	7
Polarized Sensitivity .....	8
Adaptation and Spontaneous Polarization .....	9
Proposed model for Gradient Sensing .....	10
2 MODEL FOR GRADIENT SENSING .....	15
Signal Transduction Pathway: The Phosphoinositide Cycle .....	15
Model .....	18
Receptor-ligand Binding .....	18
Adaptation Subsystem .....	19
Polarization Subsystem .....	19
Boundary and Initial Conditions .....	21
Dimensionless Equations .....	22
Model Equations .....	23
Simulations .....	24
Fast Responses .....	25
Phosphoinositide localization .....	27
Unique localization .....	29
The quasisteady state as a function of the chemoattractant stimulus .....	30
Polarized sensitivity .....	33
Slow Responses .....	38
Adaptation .....	38
Spontaneous polarization .....	39

3	MATHEMATICAL ANALYSIS .....	43
	Simplified Polarization Subsystem .....	44
	Evolution of the Phosphoinositide Localization .....	46
	First Phase .....	47
	Second Phase .....	48
	Construction of the Non-homogenous Steady State .....	48
	Outer Solution .....	49
	Inner Solution .....	56
	Zeroth Order Approximation to Complete Solution .....	59
	Instability of the Homogenous Steady State with Respect to Change in $\kappa_f$ .....	61
4	EXPERIMENTAL ANALYSIS .....	66
	The Positive Feedback Loop .....	67
	Protocols .....	71
	Culturing and Differentiation of HL60 cells .....	71
	Transient Transfection by Electroporation .....	71
	Motility Assays .....	72
	Preparation of cells .....	72
	Live cell imaging .....	72
	Fixing and Immunostaining .....	73
	Results .....	75
	Biophysical Experiments .....	75
	Spatiotemporal dynamics of gradient sensing .....	75
	Spontaneous polarization as a function of the chemoattractant concentration .....	76
	Biochemical Experiments .....	77
	Role of PI5K in the Positive Feedback Loop .....	77
	Construction of fluorescent PI5K1 $\alpha$ mutants and Coronin .....	78
	Assaying the efficacy of the fluorescent constructs in Cos7 cells .....	79
	Expression and distribution of PI5K1 $\alpha$ in dHL60 cells .....	81
	PI5K1 $\alpha$ regulates PIP <sub>3</sub> polarity in dHL60 cells .....	82
5	CONCLUSIONS .....	85
	Fast Responses .....	85
	Slow Responses .....	86

## APPENDIX

A	NOMENCLATURE .....	89
B	ORDERS OF MAGNITUDE OF PARAMETERS.....	91
	LIST OF REFERENCES .....	93
	BIOGRAPHICAL SKETCH .....	99

## LIST OF TABLES

<u>Table</u>	<u>page</u>
1-1. Models of gradient sensing.....	12
2-1. Dimensionless parameter values used in simulations.....	24
A-1. Model parameters. ....	89
A-2. Greek symbols .....	90



## LIST OF FIGURES

<u>Figure</u>	<u>page</u>
1-1. The five phases of the chemotactic cycle .....	1
1-2. Signaling involved in gradient sensing.....	3
1-3. The principle of the fluorescent imaging experiments .....	5
1-4. Simple model for localization of phosphoinositides .....	6
1-5. Schematic representation of the spatiotemporal dynamics.....	7
1-6. Dependence on pre-existing polarity .....	8
2-1. The phosphoinositide cycle .....	16
2-2. The kinetic scheme of the model.....	17
2-3. Phosphoinositide localization .....	26
2-4. Unique localization .....	29
2-5. Variation of the quasi-steady state as a function of chemoattractant stimulus.....	31
2-6. Response of a pre-existing phosphoinositide peak to a new gradient .....	34
2-7. Simulation of data in shown in Figure 1-6.. .....	36
2-8. Adaptation in response to a uniform increase in the chemoattractant concentration.....	38
2-9. Spontaneous polarization in response to a uniform but noisy chemoattractant profile. ....	40
3-1. Steady states of the reduced model.....	46
3-2. Nullcline $d\pi/d\tau = f(\pi, t) = 0$ .....	47
3-4. Phase portraits for each branch of $f(\pi, t) = 0$ .....	50
3-5. Patched phase plane for the outer solution $t(\xi)$ .....	52

3-6. Outer solution $\pi(\xi)$ .....	56
3-7. Heteroclinic orbit (AB) representing inner solution $\pi^I(y)$ .....	59
3-8. Zeroth order solutions (dashed lines) in comparison with the numerically calculated complete solution (solid lines). ....	60
3-9. Plots of $\text{Det}(M_0)$ and $\text{Trace}(M_0)$ as parameter $\kappa_f$ is varied. ....	63
3-10. Turing bifurcation of the homogenous study state .....	64
4-1. Kinetic scheme of the hypothesized positive feedback loop .....	67
4-2. Components of the positive feedback loop in a resting cell and in a polarized cell. ....	68
4-3. Spatiotemporal dynamics of PIP <sub>3</sub> localization in dHL60 cells .....	74
4-4. Spontaneous polarization as a function of chemoattractant concentration .....	76
4-5. Quantification of polarity .....	77
4-6. Distribution of endogenous PI5K1 $\alpha$ in PDGF stimulated Cos7 cells .....	79
4-7. Ruffle inhibition in PI5K1 $\alpha$ kn transfected Cos7 cells .....	79
4-8. Expression and distribution of PI5K1 $\alpha$ in dHL60 cells .....	80
4-9. Overexpression of PI5K. ....	81
4-10. Control experiment. ....	82
4-11. Inhibition of PI5K .....	83
4-12. PI5K regulation of PIP <sub>3</sub> polarization –Quantification of study .....	83

Abstract of Dissertation Presented to the Graduate School  
of the University of Florida in Partial Fulfillment of the  
Requirements for the Degree of Doctor of Philosophy

GRADIENT SENSING IN EUKARYOTIC CELLS: MECHANISM AND  
SPATIOTEMPORAL DYNAMICS

By

Kulandayan Kasi Subramanian

December 2004

Chair: Atul Narang

Cochair: Gerard P. Shaw

Major Department: Chemical Engineering

The crawling movement of cells in response to a chemical gradient is a complex process involving the orchestration of various intracellular signaling molecules. Although a complete mechanism for this process remains elusive, the very first step of gradient sensing, enabling the cell to perceive the direction of the imposed gradient, has become more transparent. The increased understanding of this step has been driven by the discovery that application of a weak chemoattractant gradient results in the localization of membrane phosphoinositides at the front end of the cell, which then acts as a “compass” for the forward motility of the cell.

Cell migration plays a pivotal role in diverse biological phenomena such as wound healing, cancer metastasis and inflammatory response. Therefore, an understanding of the gradient sensing has vast applications in the treatment of numerous human diseases.

In this dissertation, a mathematical model for gradient sensing has been formulated. This model contains a slow diffusing ‘activator’ that is synthesized autocatalytically, and

a fast diffusing 'inhibitor' that inhibits the activator. The activator and the inhibitor have been identified from the phosphoinositide signaling pathways. Such a model explains the localization of phosphoinositides in response to a chemoattractant gradient and also simulates all the other phosphoinositide dynamics observed in motile cells.

The shape of the steady state phosphoinositide localization has been analyzed by employing singular perturbation theory. This technique exploits the difference in diffusion rates between the activator and the inhibitor to analytically construct an approximation to the phosphoinositide localization. Geometric properties of the phosphoinositide localization, such as height and width have also been derived.

The stability of the homogenous phosphoinositide steady state has been analyzed. This analysis shows that the homogenous steady state of the phosphoinositides can spontaneously polarize into a phosphoinositide localization only when the phosphoinositide synthesis rate is at an optimum. This result provides an experimentally testable characteristic of the model. Two types of experiments have been done to test this hypothesis: (1) biophysical experiments that study the polarity at different uniform chemoattractant concentrations and (2) biochemical experiments that overexpress or inhibit an enzyme critical for phosphoinositide synthesis. Results of both these experiments are consistent with model predictions.

## CHAPTER 1 GRADIENT SENSING IN EUKARYOTIC CELLS

### Introduction

Directed cell migration accompanies us from conception to death.

- At birth, controlled cell migration brings about shape and organization to the embryo [1]. As the embryo develops, neurons navigate to appropriate regions of the body and direct the formation of the nervous system.
- In an adult, cell migration is indispensable for the defense and maintenance of the body. Neutrophils rapidly detect inflammation sites and engulf invading pathogens [2]. Fibroblasts under the skin move in large numbers towards wounded areas and induce healing [3].
- Cell migration can also accelerate death. Cancer metastasis is caused by directed cell migration of tumor cells from the primary site to preferential sites of metastasis [4].

Hence, a good understanding of cell migration will be able to shed light on all these biological phenomena.

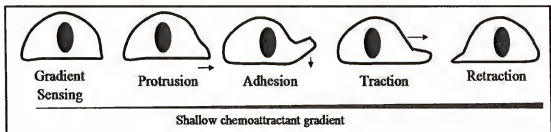


Figure 1-1. The five phases of the chemotactic cycle (adapted from [5]) (1) Gradient sensing (2) Protrusion of pseudopod (3) Adhesion to substratum (4) Traction of the cell body and (5) Retraction of the cell tail.

Most eukaryotic cells move by crawling on a surface. This crawling movement is initiated in response to an external stimulus, which is frequently a chemical concentration gradient. The resultant motion propels the cell forward along the direction of highest

concentration. The chemical that induces the movement is called chemoattractant and the movement itself is called chemotaxis [6].

Eukaryotic chemotaxis is cyclic and each cycle consists of five distinct phases (Figure 1-1) [5]. The cell first senses the external chemoattractant gradient using specialized receptive proteins on its membrane. This results in the extension of a protrusion, called a pseudopod, by polymerizing actin in the direction of maximum chemoattractant. In order to convert this response to motion, the pseudopod then adheres to the substratum. This is then followed by a contraction phase, in which the cell body and nucleus are pulled forward. The last step in locomotion consists of two distinct processes, deadhesion of the protrusion and retraction of the tail.

Each phase of the chemotactic cycle is a complex process involving the coordinated action of a large constellation of signaling molecules, many of which have been identified. Still lacking, however, is a synthetic theory explaining how these molecules are organized in space and time.

This work is primarily concerned with understanding the first phase of the cycle, gradient sensing, the mechanism that enables the cell to read the external gradient and extend a pseudopod precisely at its leading edge, the region exposed to the highest chemoattractant concentration.

The chemoattractant gradients imposed in the extracellular space are often quite small (1–2% concentration change over the length of the cell) [7], but the actin polymers, that constitute the pseudopod, are found exclusively at the leading edge [8, 9]. Thus, a key problem of gradient sensing is the elucidation of the mechanism that mediates the

formation of a highly polarized distribution of actin polymers in response to a relatively mild chemoattractant gradient.

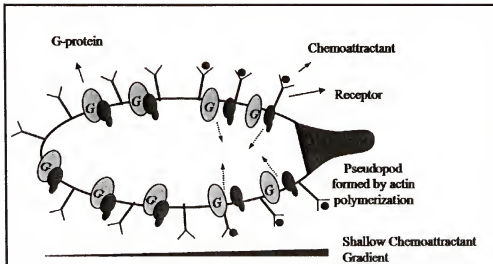


Figure 1-2. Signaling involved in gradient sensing. The chemoattractant binds to G-protein coupled receptors on the cell surface, which in turn induces the dissociation of G-proteins. Active G-proteins then propagate the signal downstream, eventually resulting in localized actin polymerization at the leading edge of the cell. In spite of a shallow external gradient, the response observed is highly localized at the leading edge of the cell.

Several cell types have been used as model systems for studying gradient sensing. They include fast moving-cells such as neutrophils [10] and the slime mold amoeba, *Dictyostelium* [11], and slow-moving cells such as neurons [12], budding yeast [13, 14] and fibroblasts [15]. Although several aspects of this work apply to slow moving cells, the primary focus will be on the fast-moving cell types.

The chemoattractant gradient is transmitted to the actin polymerization machinery by a signal transduction pathway that starts with receptors on the cell surface and terminates in proteins that catalyze actin polymerization. In *Dictyostelium* and neutrophils the receptors that regulate chemotaxis are generally G-protein coupled receptors (GPCRs). Upon ligand binding, these receptors activate heterotrimeric G-

proteins and dissociate them into  $G_{\alpha}$  and  $G_{\beta\gamma}$  subunits. Each of these subunits then activates a train of signaling events, which eventually activates proteins that catalyze actin polymerization.

It is, therefore, conceivable that actin polymers inherit their highly polarized distribution from some molecule that is upstream of the polymers in the pathway. Hence, it becomes crucial to identify the first polarized component in the chemoattractant activated signal transduction pathway. Recent experiments [15-18] have

- Shown that membrane-resident phosphoinositides, phosphatidylinositol 3,4,5-phosphate (PI(3,4,5)P<sub>3</sub>) and phosphatidylinositol 3,4 phosphate (PI(3,4)P<sub>2</sub>) are among the earliest polarized components of the signal transduction pathway involved in gradient sensing.
- Studied the spatiotemporal dynamics of these phospholipids in response to various chemoattractant profiles.

### **Identification of the First Polarized Component**

Motile cells are transfected with chimeric proteins made by fusing a fluorescent protein either to the molecule of interest or to a substance that binds specifically to the molecule of interest and thus “reports” on it. For example, the PH domain of Akt binds specifically to PI(3,4)P<sub>2</sub> and PI(3,4,5)P<sub>3</sub>, so that the fusion protein GFP-PH-Akt reports on the distribution of these phosphoinositides. A transfected cell is then exposed to a chemoattractant gradient by releasing chemoattractant from a micropipette and the resultant intracellular distribution of the fluorescent probes is visualized using fluorescence microscopy (Figure 1-3). This approach allows the study of spatial polarity at each stage of the signal transduction pathway (Figure 1-2).



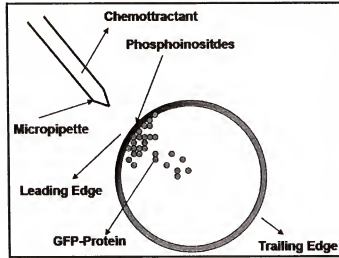


Figure 1-3. The principle of the fluorescent imaging experiments.

Specifically, it has been found that

1. **Membrane receptors are not polarized.** It was initially suggested that the localized actin polymerization could be explained by a non-uniform distribution of receptors on the cell membrane [19, 20]. However, recent studies have univocally demonstrated that when exposed to a chemoattractant gradient, receptors fail to redistribute and are in fact uniformly distributed [21, 22].
2. **Receptor occupancy and G-proteins are not significantly polarized.** Cells containing inactive G-proteins fail to chemotax [23]. Hence, receptors and G-proteins are essential for transmission of the chemoattractant signal. However, when cells are exposed to a chemoattractant gradient, the ligand bound receptors and active G-proteins show only a shallow anterior-posterior profile [24, 25]. It follows that receptors and G-proteins are required, but are not the source of the localized amplification observed at the leading edge of the cell.
3. **Phosphoinositides are significantly polarized.** Within 5-10secs of applying a chemoattractant gradient, PH domains of signaling molecules such as Akt, CRAC, PhdA and Btk strongly polarize at the edge of the cell membrane that received the strongest chemoattractant stimulus [16-18]. These PH domains report specifically on the intracellular distribution of membrane-resident phosphoinositides,  $PI(3,4)P_2$  and  $PI(3,4,5)P_3$ . In neutrophils, the gradient of these PH domains is nearly six times the chemoattractant gradient [18]. It follows that these phosphoinositides are among the earliest polarized components of the signal transduction pathway. Hereafter, this phenomenon will be referred to as phosphoinositide localization.
4. **Phosphoinositides polarize independent of the actin cytoskeleton.** The phosphoinositide localization is tightly accompanied with actin polymerization and pseudopod formation. This raised the possibility that actin polymerization is necessary for the translocation of phosphoinositides. In order to test this, a toxin

called Latrunculin A is added to depolymerize the actin and give the cell a rounded morphology. However, cells still recruited the phosphoinositides asymmetrically to the face closest to the pipette [11, 16, 18]. This showed that the localization of phosphoinositides can take place independent of the actin cytoskeleton.

Hence, the key problem in the study of gradient sensing now becomes: What is the mechanism underlying the phosphoinositide localization?

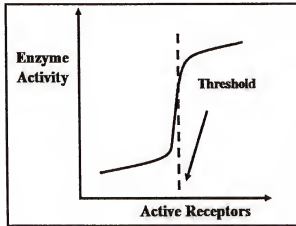


Figure 1-4. Simple model for localization of phosphoinositides. The activity of the enzyme that synthesizes phosphoinositides is a sharp non-linear function of the active receptors. Any shallow chemoattractant gradient centered around the threshold would yield a large phosphoinositide gradient. This model shows that the phosphoinositide response is simply an amplified version of the chemoattractant gradient.

At first sight, the localization of phosphoinositides seems explicable in terms of a simple amplification model. It suffices to postulate that the phosphoinositide synthesis responds to receptor activation in a highly cooperative manner (Hill-type kinetics) (see Figure 1-4). In this case, the phosphoinositide distribution will be similar in shape, but steeper in slope, when compared to the chemoattractant concentration profile. In other words, the phosphoinositide distribution is an amplified version of the chemoattractant concentration profile. However, several experiments show that eukaryotic gradient sensing is not a matter of simple amplification. In each of the experiments below, the

distribution of the phosphoinositide localization differs from the chemoattractant profile imposed on the cell.

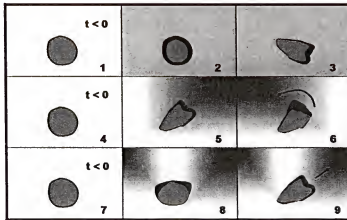


Figure 1-5. Schematic representation of the spatiotemporal dynamics. *Upper panel:*

When a resting cell (shown in 1) is exposed to a uniform increase in chemoattractant concentration, it immediately responds by increasing phosphoinositides all over the membrane (shown in 2). This is followed by the spontaneous polarization (shown in 3) of phosphoinositides along a random direction. *Middle panel:* When a resting cell (shown in 4) is exposed to a gradient of chemoattractant, it accumulates phosphoinositides at the point of highest chemoattractant concentration (shown in 5). When the direction of the gradient is switched the existing localization turns in the direction of the new source of chemoattractant (shown in 6). This phenomenon is called polarized sensitivity. *Lower panel:* When a resting cell (shown in 7) is exposed to two unequal chemoattractant sources, it responds to both sources initially. However, as time progresses the response to the stronger source grows and the response to the weaker source is completely abolished. We refer to this as unique localization.

### Spatiotemporal Dynamics

Motile cells are exposed to a variety of chemoattractant profiles which include (1) steady or time varying gradients produced by releasing chemoattractant from one or more chemoattractant sources and (2) steady uniform profiles obtained by immersing the cell in chemoattractant. These experiments result in the manifestation of the following spatiotemporal dynamics (see Fig 1-5): (1) unique localization (2) polarized sensitivity (3) adaptation and (4) spontaneous polarization. In the following section, these dynamics

will be defined precisely by describing the experiments and the corresponding observations.

### Unique Localization

In normal motile cells, only one leading edge ultimately develops, regardless of the external signal. Foxman et al., 1997, provided a convincing demonstration of this behavior by exposing a cluster of motile cells to two chemoattractant sources located at different distances from the cluster. All the cells migrated towards the closer source, showing that cells respond to the stronger stimulus and completely ignore the weaker stimulus. This phenomenon is referred to as unique localization.

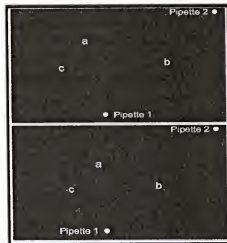


Figure 1-6. Dependence on pre-existing polarity. Response of three cells labeled *a*, *b*, and *c* to sequential stimulation by two chemoattractant sources (from [26]). The top panel shows all three cells moving towards the sole chemoattractant source (pipette 1). The bottom panel shows the response when an additional source (pipette 2) is turned on some time later. Cell '*a*' immediately turns toward pipette 2, whereas cells '*b*' and '*c*' show no response at all.

### Polarized Sensitivity

If a cell that has localized phosphoinositides in a certain direction is exposed to a modest chemoattractant gradient along a different direction, a new localization does not develop at the point with the highest chemoattractant concentration. Instead, the existing

localization turns and reorients itself along the new gradient. This phenomenon is called polarized sensitivity, since the turning response suggests that pre-existing leading edge or “pole” is more sensitive to chemotactic signals than all other regions of the cell.

Interestingly, if the new chemoattractant gradient is relatively large and localized, the existing pseudopod retracts and a new one grows along the direction of the new gradient.

The induction of a turning response depends not only on the external concentration, but also on the preexisting polarity of the cell. This is dramatically illustrated by an experiment shown in Figure 1-6 [26]. The upper panel shows three cells labeled *a*, *b* and *c* moving toward the chemoattractant source shown as pipette 2. Interestingly, even though cell *b* is much closer to pipette 2 than cell *a*, it does not respond at all, whereas the more distant cell *a* turns toward pipette 2. This shows that the cells *b* and *c* that are closer to pipette 1, and hence likely to be more polarized, are less responsive to the subsequent influence of pipette 2.

### **Adaptation and Spontaneous Polarization**

When resting cells are stimulated with a uniform chemoattractant concentration, the phosphoinositides in the membrane increase uniformly within 5–10 seconds. However, if this uniform concentration is maintained at the same level, the phosphoinositides decrease to their prestimulus steady state [11, 16]. This phenomenon is called adaptation [27]. The mechanism underlying adaptation is only partially understood.

In *Dictyostelium*, earlier work showed that adaptation was perfect, i.e., the membrane phosphoinositides returned to their basal steady state [16]. However, recent work shows that cells frequently form multiple patches of phosphoinositide localization, instead of completely adapting to their prestimulus state, suggesting that adaptation is in fact imperfect [28].

Adaptation is manifested in a slightly different manner in neutrophils [29]. After exhibiting a uniform initial increase, the phosphoinositides spontaneously localize at a random location on the membrane and decrease at all other regions of the cell [18, 30]. The region of phosphoinositide localization subsequently becomes the leading edge of the cell. This phenomenon is called spontaneous polarization to emphasize the fact that the phosphoinositides and the cell morphology polarize even though the chemoattractant environment is macroscopically uniform [14]. The time taken for the initial, uniform increase is independent of the chemoattractant concentration [29]. However, the amplitude of the initial response and the time taken for the spontaneous polarization to occur is directly proportional to the chemoattractant concentration.

#### **Proposed model for Gradient Sensing**

From the dynamics discussed above, it is possible to discern essential components for a model of gradient sensing. A large accumulation of membrane phosphoinositides at the leading edge implies that the external chemoattractant signal is being amplified. The lack of a response at low concentrations of chemoattractant implies the existence of a threshold below which there is no amplification. These properties are exhibited in systems containing an activator, a substance that produces more of itself (ensures amplification) and possesses co-operative kinetics (ensures a threshold for amplification).

A model consisting of only an activator cannot exhibit a localized response. When sub-threshold perturbations are applied, the system comes back to the original homogenous steady state. On the other hand when supra-threshold, localized perturbations are applied to such a system, the activator is autocatalytically produced at the site of the perturbation and will diffuse freely in order to ultimately reach a uniformly

high activator profile. The localized response can only be achieved by limiting the uncontrolled propagation of the activator, using a component called the inhibitor.

This leads us to consider a Gierer and Meinhardt type activator-inhibitor model [31] that allows for the formation of a stable pattern. This model consists of two variables – an activator and an inhibitor. An activator enhances production of itself and the production of the inhibitor. An inhibitor enhances production of itself and inhibits the production of the activator. The most general form of the model is as follows

$$\text{Activator: } \frac{\partial a}{\partial t} = f(a, i) + D_a \frac{\partial^2 a}{\partial x^2} \quad (1.1)$$

$$\text{Inhibitor: } \frac{\partial i}{\partial t} = g(a, i) + D_i \frac{\partial^2 i}{\partial x^2} \quad (1.2)$$

where  $f(a, i)$  and  $g(a, i)$  express the rate of formation of the activator and the inhibitor.

$D_a$  and  $D_i$ , denote the lateral diffusivities of the activator and inhibitor, respectively. Let us assume that both variables are initially at a homogenous steady state and that a supra-threshold perturbation is given at a random location in space. If the diffusion coefficients of both these components are of the same order ( $D_a \approx D_i$ ), localized production of the activator is inhibited by the production of inhibitor at the very same region. Again, a non-uniform steady state ceases to exist. Gierer and Meinhardt [31] proposed that the localization of the activator is possible only if the inhibitor is much faster diffusing than the activator ( $D_i \gg D_a$ ). In this case, the inhibitor would immediately diffuse away the site of the perturbation. This rapid diffusion of the inhibitor has a two-fold effect: (a) It allows for the amplification of the activator at the site of the perturbation. (b) It increases the inhibitory effect away from the perturbation site, and prevents the build up of the

activator. This results in the stable localization of the activator at the perturbation site. Turing [32], was the first to discover the diffusion driven instability of the homogenous steady state.

Table 1-1. Models of gradient sensing.

Model	Spatiotemporal dynamics				
	Localization	Adaptation	Spontaneous polarization	Polarized sensitivity	Unique localization
[33]	✓		✓	✓	
[34]	✓	✓			
[35]	✓	✓			
[36, 37]	✓	✓			
[38]	✓	✓			✓
[39]	✓	✓	✓	✓	✓

The desire to capture the spatiotemporal dynamics of the phosphoinositides has spurred the development of several mathematical models. Each of these models present elegant mechanisms that can explain some of the dynamics of gradient sensing. However, none of these models, except for the model described in this work [39], have predicted all of the spatiotemporal dynamics. Table 1-1 shows a comparison of these models with respect to the spatiotemporal dynamics that they exhibit.

Three of these models contain a short-range activator that is synthesized autocatalytically, and a long-range inhibitor that inhibits the synthesis of the activator [33-35]. They differ only with respect to the postulated mechanisms of the activation and inhibition and the dynamics that have been explained. Two other models contain a long-range inhibitor but no activator; i.e., there is no autocatalytic synthesis [36-38]. These two models differ with respect to the reaction kinetics — the synthesis rate of the inhibitor is rapid in the first case, and slow in the second case. Recently, Haugh and



coworkers [40, 41], have proposed a model for fibroblast gradient sensing based on the turnover and diffusion of a single intracellular component.

This dissertation has been organized in the following manner. In Chapter 2, a signaling pathway called the phosphoinositide cycle has been proposed for gradient sensing. Candidates for activator and inhibitor have been identified from this signaling pathway. Based on these assumptions, a mathematical model for gradient sensing has been formulated. This model has been used to simulate the phosphoinositide dynamics observed when the cell is exposed to various types of chemoattractant profiles. Specifically, the manifestation of five distinct types of dynamics: (1) phosphoinositide localization (2) unique localization (3) polarized sensitivity (4) adaptation and (5) spontaneous polarization, have been explained using this model. These results suggest that an activator-inhibitor type mechanism is in fact consistent with the dynamics of gradient sensing.

Chapter 3 describes the analytical construction of the phosphoinositide localization. This analysis exploits the difference in diffusion rates of the activator and the inhibitor, to construct a zeroth order approximation to the phosphoinositide localization. Geometric properties of the phosphoinositide localization, such as height and width have also been derived. Chapter 3 also discusses the stability of the homogenous resting state of the phosphoinositides with respect to small non-homogenous perturbations. This analysis allows us to determine the conditions under which the homogenous steady state spontaneously polarizes into a phosphoinositide localization.

The results of the model simulations, in Chapter 2, show that the width of the phosphoinositide localization changes with the rate of phosphoinositide synthesis. This

provides a simple way to experimentally test the model that has been formulated for gradient sensing. Chapter 4 describes these experiments that have been performed on a neutrophil cell line. Specifically, two types of experiments have been performed: a) biophysical experiments, where the extent of polarity has been studied at various mean concentrations of chemoattractant and b) biochemical experiments, in which the activity of the enzyme that synthesizes phosphoinositides has been manipulated to verify if the rate of phosphoinositide synthesis can influence phosphoinositide polarization. The results of both these experiments turn out to be consistent with the hypothesized model.

## CHAPTER 2 MODEL FOR GRADIENT SENSING

Many of the signaling components involved in gradient sensing have been identified. However, the exact mechanism underlying this process remains unclear. The simple model formulated in this work, reproduces nearly all the spatiotemporal dynamics observed during gradient sensing. The model is based on a signal transduction pathway called the phosphoinositide cycle. Although the role of this pathway in gradient sensing has not been comprehensively established, the success of this remarkably concise model suggests that the molecular players, whatever is their identity, probably possess the properties of the variables in the model. Hence, the model can help identify the type of reaction network that could give rise to the observed dynamics.

### **Signal Transduction Pathway: The Phosphoinositide Cycle**

The signaling pathway that follows receptor activation is the subject of ongoing research. In *Dictyostelium discoideum* and neutrophils, receptor-ligand binding activates heterotrimeric G-proteins. Activated G-proteins can activate PI3K<sup>1</sup> by direct binding [42], resulting in the synthesis of PIP<sub>3</sub> from PIP<sub>2</sub> (see Figure 2-1). The PIP<sub>3</sub> thus produced and the G $\beta\gamma$  subunit then synergistically activates the membrane-resident protein, P-Rex1 [43-45], which belongs to the Dbl family Rac-GEFs (guanine-nucleotide

---

<sup>1</sup> Abbreviations Used: PI, phosphatidylinositol; PIP, phosphatidylinositol 4-phosphate; PIP<sub>2</sub>, phosphatidylinositol 4,5-phosphate; PIP<sub>3</sub>, phosphatidylinositol 3,4,5-phosphate; DG, diacylglycerol; IP<sub>3</sub>, inositol 1,4,5-triphosphate; PI3K, phosphatidylinositol 3-kinase; PI5K, phosphatidylinositol 4-phosphate 5-kinase; PITP, phosphatidylinositol transport protein; Prex1, PIP<sub>3</sub>-dependent Rac exchanger

exchange factors for Rac) that activate Rac. Activated P-Rex1 then converts the inactive Rac-GDP to active Rac-GTP.

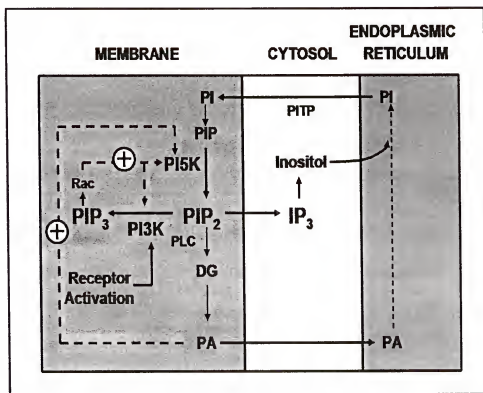


Figure 2-1. The phosphoinositide cycle.

There is growing evidence that Rac mediates activation of both PI3K and PI5K [46, 47]. This has led to the suggestion that PIP<sub>3</sub> and Rac function in a positive feedback loop for more synthesis of PIP<sub>2</sub> and PIP<sub>3</sub> [34, 48, 49]. Activation of PI5K creates yet another positive feedback loop because this increases the synthesis rate of PIP<sub>2</sub> and its downstream product, phosphatidic acid (PA), a potent activator of PI5K [50]. Because of these two positive feedback loops, the synthesis rate of PIP<sub>2</sub> and PIP<sub>3</sub> can rapidly accelerate to high levels.

Such high synthesis rates of PIP<sub>2</sub> and PIP<sub>3</sub> can be sustained for no more than a second because the concentration of phosphatidylinositol (PI) in the plasma membrane is



of the cell. In addition, it has been shown that  $PIP_2$ , in conjunction with GTP-bound Cdc42, is a strong activator of N-WASP, which in turn activates Arp2/3 [59]. Similarly, Rac activation and  $PIP_3$  production activate WAVE proteins, which can also activate Arp2/3 [59]. Activated Arp2/3 mediates actin polymerization by nucleating the sides of pre-existing actin filaments [60]. Actin polymerization by Arp2/3 is believed to drive lamellipod protrusion [61]. Taken together, these facts suggest that the localization of  $PIP_2$  and  $PIP_3$  resulting from the gradient sensing mechanism plays a crucial role in the subsequent extension of the lamellipod.

### Model

Figure 2-2 shows the structure of the model. The extracellular signal is received by the receptor and transmitted sequentially to the adaptation and polarization subsystems. In earlier work [34], adaptation was modeled by assuming slow desensitization and resensitization of receptors. In view of the subsequent observations concerning the locus of adaptation in the signaling pathway [25, 62], it has been assumed that the adaptation subsystem lies below the receptors and above the polarization subsystem.

### Receptor-ligand Binding

It is assumed that diffusion of receptors is negligibly small and receptor-ligand binding follows the mass action law. The concentration of ligand-bound (active) receptors, denoted, is then given by

$$\frac{\partial r}{\partial t} = k^+(r_t - r)l - k^-r \quad (2.1)$$

where  $k^+$  and  $k^-$  are the rate constants for association and dissociation, respectively;  $r_t$  is the total concentration of receptors; and  $l$  is the ligand concentration.

### Adaptation Subsystem

The molecular mechanism of adaptation is unknown. However, since the interest lies in studying the effect of adaptation on the dynamics of amplification, a simple ‘toy’ adaptation model formulated by [27] will suffice. This model encapsulates the key properties of adaptation. It consists of two variables  $\mu$  and  $\vartheta$  that do not diffuse and evolve according to the equations

$$\left(\frac{1}{a}\right)\frac{\partial\mu}{\partial t} = \rho - \mu - \vartheta \quad (2.2)$$

$$\left(\frac{1}{b}\right)\frac{\partial\vartheta}{\partial t} = \rho - \vartheta \quad (2.3)$$

where  $\mu, \vartheta$  are the dimensionless concentrations of two hypothetical entities,  $U, V$ ;  $\rho \equiv r/r_i$  is the fraction of ligand-bound receptors;  $1/a, 1/b$  are the time constants for the evolution of  $\mu$  and  $\vartheta$ . It is assumed that the dynamics of  $U$  are much faster than the dynamics of  $V$ , i.e.,  $a \gg b$ . Equations (2.2–2.3) comprise the adaptation subsystem of the model. This subsystem is only capable of predicting perfect adaptation. Although the adaptation subsystem has no biochemical relevance, it can effectively simulate the dynamics of adaptation. Given any active receptor distribution,  $\rho$ , the steady state concentration of  $U$  always approaches zero. Inasmuch as the polarization subsystem “sees” the extracellular environment through the variable  $U$  (Figure 2-2), it becomes blind to it after a sufficiently large time interval. The effects of such a property on the dynamics of polarization will be studied.

### Polarization Subsystem

To capture the spatiotemporal dynamics described earlier, the adaptation subsystem will be coupled to the polarization subsystem. The polarization subsystem is an

abstraction of the phosphoinositide cycle (Figure 2-2). It contains three variables corresponding to three “lumped” pools, namely, membrane phosphoinositides ( $P$ ), cytosolic inositol and its phosphates ( $I$ ), and phosphoinositides in the endoplasmic reticulum ( $P_s$ ). The concentrations of these variables are denoted by  $p$ ,  $i$  and  $p_s$ , respectively. It is assumed that

- The cell is two-dimensional and disk-shaped. Thus,  $p$  and  $p_s$  are based on the length of the plasma membrane and  $i$  is based on the area of the cytosol.
- Radial gradients of the cytosolic inositol phosphate pool are negligibly small. This is reasonable because inositol phosphates diffuse rapidly. However, angular gradients of this pool are considered because membrane phosphoinositides, being slow diffusers, develop steep angular gradients. These sharp gradients could induce mild angular gradients of inositol phosphates.
- There is basal synthesis and degradation of  $P$  and  $I$ . Basal synthesis rates of  $P$  and  $I$ , denoted  $c_p$  and  $c_i$ , follow zero-order kinetics. Basal degradation rates, denoted  $r_{p,d}$  and  $r_{i,d}$ , obey first-order kinetics with rate constants  $k_p$  and  $k_i$ , respectively, i.e.,

$$r_{p,d} \equiv k_p p, r_{i,d} \equiv k_i i$$

- The receptor-mediated rate of formation of membrane phosphoinositides per unit length of membrane is given by

$$r_{p,f} \equiv k_f \mu p^2 p_s$$

where  $k_f$  is the rate constant and  $\mu$  is the dimensionless concentration of  $U$ . Here, we have assumed that  $U$  induces phosphoinositide synthesis by activating PI3K. The dependence on  $p^2$  represents the autocatalytic and cooperative kinetics with respect to membrane phosphoinositides. This is an idealization of the two positive feedback loops shown in Figure 2-1. The membrane phosphoinositides will play the role of a local activator in the model.

- The inositol phosphate pool ( $I$ ) stimulates transfer of phosphoinositides from the plasma membrane to the endoplasmic reticulum. The rate of removal of membrane phosphoinositides per unit length of the membrane is assumed to be

$$r_{p,r} \equiv k_r p i$$



where  $k_r$  denotes the rate constant. The rationale for this assumption is as follows. Inositol reacts with CDP.DG to regenerate PI in the endoplasmic reticulum (Figure 2-1). An increase in inositol levels, therefore, promotes this reaction and drives the transfer of PA from the plasma membrane to the endoplasmic reticulum. Thus, the rate of removal of membrane phosphoinositides depends on  $p$  and should also depend on the concentration of the inositol phosphates,  $i$ . The inositol phosphates will act as a global inhibitor.

The dynamics of  $P$ ,  $P_s$  and  $I$  are then governed by the equations

$$\frac{\partial P}{\partial t} = k_f \mu p^2 P_s - k_r p i + c_p - k_p P + \frac{D_p}{R^2} \frac{\partial^2 P}{\partial \theta^2} \quad (2.4)$$

$$\frac{\partial P_s}{\partial t} = -(k_f \mu p^2 P_s - k_r p i + c_p - k_p P) + \frac{D_{P_s}}{R^2} \frac{\partial^2 P_s}{\partial \theta^2} \quad (2.5)$$

$$\frac{\partial i}{\partial t} = s(k_f \mu p^2 P_s - k_r p i) + c_i - k_i i + \frac{D_i}{R^2} \frac{\partial^2 i}{\partial \theta^2} \quad (2.6)$$

where  $D_p$ ,  $D_{P_s}$  and  $D_i$  denote the lateral diffusivities of  $P$ ,  $P_s$  and  $I$ , respectively, and  $R$  denotes the cell radius. The factor  $s$ , which denotes the membrane length per unit cell area, is required since synthesis and removal rates of  $P$  are based on the length of the plasma membrane.

The complete model accounting for receptor-ligand binding, adaptation and spatial sensing consists of equations (2.1–2.6). It remains to specify the boundary and initial conditions.

### Boundary and Initial Conditions

Since the cell is disc-shaped, all the variables satisfy periodic boundary conditions; that is

$$x(0, \tau) = x(1, \tau), \frac{\partial x(0, \tau)}{\partial \xi} = \frac{\partial x(1, \tau)}{\partial \xi}, \tau > 0$$

where  $x \equiv r, \mu, \vartheta, p, P_s, i$ . For future use, note that (2.4–2.5) and the boundary conditions imply that the total amount of phosphoinositides in the plasma membrane and the

endoplasmic reticulum,  $\int_0^{2 \times 3.1416} (p + p_s) R d\theta$ , is conserved. Hence, the average concentration of phosphoinositides in the cell

$$p_t \equiv \frac{1}{C} \int_0^{2 \times 3.1416} (p + p_s) R d\theta, C \equiv \text{circumference of the cell}$$

is constant. The initial distribution of a variable will be denoted by appending the superscript ‘-’ to the variable. Thus

$$\begin{aligned} r(0, \theta) &= r^-, \mu(0, \theta) = \mu^-, g(0, \theta) = g^- \\ p(0, \theta) &= p^-, p_s(0, \theta) = p_s^-, i(0, \theta) = i^-, 0 \leq \theta < 2 \times 3.1416 \end{aligned}$$

Various initial distributions have been used in the simulations. They are specified before the description of each of the simulations.

### Dimensionless Equations

Using the dimensionless variables

$$\rho \equiv \frac{r}{r_t}, \pi \equiv \frac{p}{p_t}, \pi_s \equiv \frac{p_s}{p_t}, t \equiv \frac{i}{s p_t}, \mathcal{E} \equiv \frac{\theta}{2 \times 3.1416}, \tau \equiv \frac{t}{1/(k_r s p_t)}$$

and dimensionless parameters,

$$\begin{aligned} \tau_r &\equiv \frac{k_r s p_t}{k^-} & \tau_u &\equiv \frac{k_r s p_t}{a} & \tau_v &\equiv \frac{k_r s p_t}{b} & \kappa_p &\equiv \frac{k_p}{k_r s p_t} \\ \delta_p &\equiv \frac{D_p / C^2}{k_r s p_t} & \delta_{p_s} &\equiv \frac{D_{p_s} / C^2}{k_r s p_t} & \psi_p &\equiv \frac{c_p p_t}{k_r s p_t} & \kappa_i &\equiv \frac{k_i}{k_r s p_t} \\ \delta_i &\equiv \frac{D_i / C^2}{k_r s p_t} & \kappa_f &\equiv \frac{k_f p_t^2}{k_r s p_t} & \psi_i &\equiv \frac{c_i p_t}{k_r s p_t} & \lambda &\equiv \frac{l}{k^+ / k^-} \end{aligned}$$

the following dimensionless equations

$$\tau_r \frac{\partial \rho}{\partial \tau} = (1 - \rho) \lambda - \rho$$

$$\tau_u \frac{\partial \mu}{\partial \tau} = \rho - \mu - g$$

$$\tau_v \frac{\partial g}{\partial \tau} = \rho - g$$

$$\begin{aligned}\frac{\partial \pi}{\partial \tau} &= \kappa_f \mu \pi^2 \pi_s - \pi l + \psi_p - \kappa_p \pi + \delta_p \frac{\partial^2 \pi}{\partial \xi^2} \\ \frac{\partial \pi_s}{\partial \tau} &= -\left(\kappa_f \mu \pi^2 \pi_s - \pi l + \psi_p - \kappa_p \pi\right) + \delta_p \frac{\partial^2 \pi_s}{\partial \xi^2} \\ \frac{\partial l}{\partial \tau} &= \kappa_f \mu \pi^2 \pi_s - \pi l + \psi_l - \kappa_l l + \delta_l \frac{\partial^2 l}{\partial \xi^2}\end{aligned}$$

dimensionless boundary conditions

$$\begin{aligned}x(0, \tau) &= x(1, \tau), \frac{\partial x(0, \tau)}{\partial \xi} = \frac{\partial x(1, \tau)}{\partial \xi}, \tau > 0 \\ x &\equiv \rho, \mu, \nu, \pi, \pi_s, l\end{aligned}$$

and dimensionless initial conditions can be obtained.

$$\begin{aligned}\rho(0, \xi) &= \rho^-, \mu(0, \xi) = \mu^-, \nu(0, \xi) = \nu^-, \pi(0, \xi) = \pi^- \\ \pi_s(0, \xi) &= \pi_s^-, l(0, \xi) = l^-, 0 \leq \xi < 1\end{aligned}$$

### Model Equations

The activation of receptors and PI3K is assumed to fast compared to amplification, i.e.,  $\tau_r, \tau_u \ll 1$ . Hence,  $\rho$  and  $\mu$  instantly achieve the quasisteady state concentrations. The dynamics for all but the smallest initial time intervals are then approximated by the equations

$$\rho = \frac{\lambda}{1 + \lambda} \quad (2.7)$$

$$\mu = \rho - \vartheta = \frac{\lambda}{1 + \lambda} - \vartheta \quad (2.8)$$

$$\tau_v \frac{\partial \vartheta}{\partial \tau} = \rho - \vartheta = \frac{\lambda}{1 + \lambda} - \vartheta \quad (2.9)$$

$$\frac{\partial \pi}{\partial \tau} = \kappa_f \mu \pi^2 \pi_s - \pi l + \psi_p - \kappa_p \pi + \delta_p \frac{\partial^2 \pi}{\partial \xi^2} \quad (2.10)$$

$$\frac{\partial \pi_s}{\partial \tau} = -(\kappa_f \mu \pi^2 \pi_s - \pi t + \psi_p - \kappa_p \pi) + \delta_{p_i} \frac{\partial^2 \pi_s}{\partial \xi^2} \quad (2.11)$$

$$\frac{\partial t}{\partial \tau} = \kappa_f \mu \pi^2 \pi_s - \pi t + \psi_i - \kappa_i t + \delta_i \frac{\partial^2 t}{\partial \xi^2} \quad (2.12)$$

the boundary conditions

$$x(0, \tau) = x(1, \tau), \frac{\partial x(0, \tau)}{\partial \xi} = \frac{\partial x(1, \tau)}{\partial \xi}, \tau > 0, x \equiv \nu, \pi, \pi_s, t \quad (2.13)$$

and initial conditions

$$\mathcal{G}(0, \xi) = \mathcal{G}^-, \pi(0, \xi) = \pi^-, \pi_s(0, \xi) = \pi_s^-, t(0, \xi) = t^-, 0 \leq \xi < 1 \quad (2.14)$$

### Simulations

The simulations have been done using the NAG subroutine D03PHF [63]. The parameter values used in the simulations are shown in Table 2-1. The rationale for the choice of parameter values can be found in Appendix B. To facilitate comparison of the simulations with experimentally observed dynamics, it is useful to note that  $k_r sp_i \sim 1/\text{sec}$ .

Table 2-1. Dimensionless parameter values used in simulations.<sup>2</sup>

$\tau_r = 0.1$	$\tau_u = 0.1$	$\tau_v = 1000$
$\delta_i = 1$	$\delta_p = 0.001$	$\delta_{p_s} = 0.001$
$\kappa_f = 6$	$\kappa_i = 0.1$	$\psi_i = 0.01$
$\phi_i = 7.67 \times 10^{-7}$	$\kappa_p = 0.1$	$\psi_p = 0.01$

Therefore, each unit<sup>3</sup> of the dimensionless time,  $\tau$ , corresponds to roughly 1sec.

Since the time scale of adaptation is on the order of minutes, we assume that  $\tau$ , i.e.,

adaptation is slow compared to the reactions involved in amplification.

---

<sup>2</sup> The choice of parameter values and the nomenclature for the greek symbols are discussed in the Appendix.

Hence, the motion after PI3K activation, which is governed by equations (2.7–2.14), can be decomposed into two phases.

1. During the first phase, there is no adaptation. Thus,  $\mathcal{G}$  remains constant at its initial value,  $\mathcal{G}^-$ , and  $\pi, \pi_s, i$  evolve towards their quasisteady state.
2. During the second phase, the effects of adaptation become perceptible, so that  $\mathcal{G}$  moves slowly towards its steady state value  $\rho$ , while  $\pi, \pi_s, i$  remain at their quasisteady state values.

These shall be referred to as the fast response and slow response, respectively. Five distinct types of spatiotemporal dynamics were described earlier. Three of them, phosphoinositide localization, polarized sensitivity and unique localization, can be completely understood by confining attention to the fast response. To understand the remaining two responses, adaptation and spontaneous polarization, the entire transient, consisting of the fast and the slow response, must be considered.

### Fast Responses

The fast response is described by the equations

$$\mu = \frac{\lambda}{1 + \lambda} - \mathcal{G}^- \quad (2.15)$$

$$\frac{\partial \pi}{\partial \tau} = \kappa_f \mu \pi^2 \pi_s - \pi i + \psi_p - \kappa_p \pi + \delta_p \frac{\partial^2 \pi}{\partial \xi^2} \quad (2.16)$$

$$\frac{\partial \pi_s}{\partial \tau} = -(\kappa_f \mu \pi^2 \pi_s - \pi i + \psi_p - \kappa_p \pi) + \delta_p \frac{\partial^2 \pi_s}{\partial \xi^2} \quad (2.17)$$

$$\frac{\partial i}{\partial \tau} = \kappa_f \mu \pi^2 \pi_s - \pi i + \psi_i - \kappa_i i + \delta_i \frac{\partial^2 i}{\partial \xi^2} \quad (2.18)$$

with boundary conditions

---

<sup>3</sup> In Dictyostelium, adaptation is observed within 50secs[16]. This time scale can be accommodated by assuming  $k_s p_i \sim 10/\text{sec}$ . In this case, each unit of  $\tau$  corresponds to roughly 0.1sec.

$$x(0, \tau) = x(1, \tau), \frac{\partial x(0, \tau)}{\partial \xi} = \frac{\partial x(1, \tau)}{\partial \xi}, \tau > 0, x \equiv \pi, \pi_s, l \quad (2.19)$$

and initial conditions

$$\pi(0, \xi) = \pi^-, \pi_s(0, \xi) = \pi_s^-, l(0, \xi) = l^-, 0 \leq \xi < 1 \quad (2.20)$$

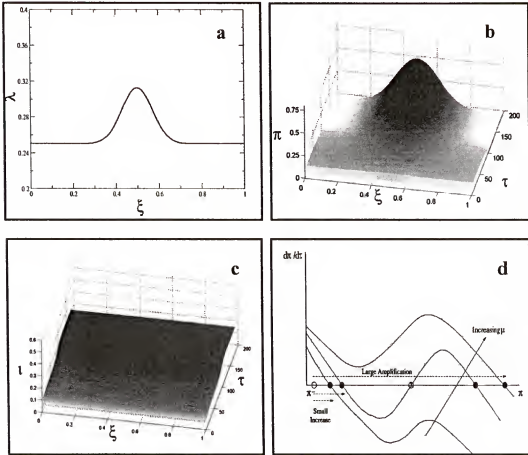


Figure 2-3. Phosphoinositide localization. (a) Chemoattractant concentration profile at  $\tau \geq 0$  (b) Development of a pronounced membrane phosphoinositide peak at  $\xi = 1/2$  which corresponds to the leading edge of the cell (c) Growth of the uniformly distributed inositol phosphate pool (d) Initial dynamics of membrane phosphoinositides at any point of the cell membrane with  $\mu$  at that point as a control parameter. When  $\mu$  is small, the existence of a stable lower steady state prevents amplification of all sufficiently small perturbations of  $\mu$ . At sufficiently large values of  $\mu$ , the lower and intermediate steady states vanish resulting in the disappearance of the threshold and the amplification of  $\mu$ .

### Phosphoinositide localization

The experiments show that when a resting cell is exposed to a chemoattractant gradient, phosphoinositides polarize within a few seconds. To simulate this experiment, assume that at  $\tau < 0$ , the cell is at the resting steady state, ie., the steady state obtained in the absence of exogenous chemoattractant ( $\lambda = 0$ ). Hence,  $\mu^-$ ,  $\mathcal{G}^- = 0$  and  $\pi^-, \pi_s^-, i^-$  are constants satisfying the equations

$$0 = \psi_p - \pi i - \kappa_p \pi$$

$$0 = \psi_i - \pi i - \kappa_i i$$

$$\pi_s = 1 - \pi$$

At  $\tau \geq 0$ , a chemoattractant gradient,  $\lambda(\xi)$ , is applied. The subsequent evolution of  $\pi$ ,  $\pi_s$  and  $i$  is then obtained by integrating (2.15–2.20) with  $\mathcal{G}^-, \pi^-, \pi_s^-, i^-$  as determined by the foregoing equations.

Figure 2-3a shows the chemoattractant profile,  $\lambda(\xi)$ , imposed at  $\tau \geq 0$ . Despite the mild chemoattractant gradient, the simulation shows that a pronounced phosphoinositide peak develops at  $\xi = 1/2$  which corresponds to the leading edge of cell (Figure 2-3b). Compared to the strongly polarized distribution of membrane phosphoinositides, the concentration profile of inositol phosphates is virtually flat (Figure 2-3c).

An intuitive explanation of these dynamics can be given by observing that when the cell is at its resting steady state, there is a threshold for peak formation. To see this, perturb the profile of  $\mu$  from its initial uniform distribution,  $\mu^-$ , to a nonuniform distribution,  $\mu(\xi)$ . Immediately after the perturbation,  $\pi_s \approx \pi_i^- = 1 - \pi$  and  $i \approx i^-$ . Moreover, since the initial concentration gradients are small, diffusion plays no role.

Hence, the initial phosphoinositide dynamics at any point of the membrane may be approximated by

$$\frac{\partial \pi}{\partial \tau} = \kappa_f \mu \pi^2 (1 - \pi) - \pi i^- + \psi'_p - \kappa_p \pi \quad (2.21)$$

Figure 2-3d shows the dynamics of this equation for various values of  $\mu$ . If  $\mu$  is small, there is either a low steady state or bistable steady states. In the first case,  $\pi$  is stably maintained at the lower steady state and in the second case, the intermediate steady state acts as a threshold that prevents a significant increase in  $\pi$ . However, if  $\mu$  is large enough at a point, the two lower steady states disappear and every  $\pi^-$  gets amplified to the upper steady state. Similarly, an increase in  $i^-$  decreases  $\pi$  to the lower steady state and a decrease in  $i^-$  allows for the amplification of  $\pi$  to the upper steady state.

The formation of the phosphoinositide peak can now be explained as follows. If  $\mu(\xi)$  is sufficiently large, the threshold vanishes and the concentration of  $P$  starts increasing at all points on the membrane. However, this increase in  $P$  does not persist at the trailing edge of the cell. It is contained by the rapid diffusion of the cytosolic inositol phosphates ( $I$ ) being produced at the leading edge. The rapid diffusion of  $I$  has a two-fold effect. In the neighborhood of the leading edge, the inhibitory effect of  $I$  is diminished. In other words,  $I$  is not high enough to inhibit the autocatalytic formation of  $P$  at the leading edge. Outside this neighborhood, the higher concentration of  $I$  promotes transfer of membrane phosphoinositides from the plasma membrane to the endoplasmic reticulum. The net effect of this transfer is to deplete the plasma membrane of its phosphoinositides, thus preventing the peak from spreading beyond the leading



edge. Hence, within the leading edge, the steady state concentration of  $P$  is higher than the initial basal level. Outside the leading edge, it is lower than the initial basal level.

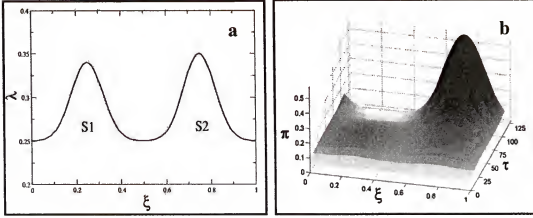


Figure 2-4. Unique localization (a) Chemoattractant profile at  $\tau \geq 0$ . The source  $S_2$  is slightly stronger than the source  $S_1$ . (b) The evolution of the corresponding phosphoinositide distribution. A pronounced phosphoinositide peak develops at the site of source  $S_2$ .

### Unique localization

The experiments show that cells can discriminate between two chemoattractant sources. Specifically, when cells encounter two chemoattractant sources of unequal strengths, they migrate toward the stronger source. The simulations show that the model cell discriminates between two sources of almost identical strengths.

To this end, assume that a resting cell is exposed to a chemoattractant profile,  $\lambda(\xi)$ , arising from two chemoattractant sources,  $S_1$  and  $S_2$ , of almost identical strengths located at  $\xi_1$  and  $\xi_2$ , respectively (Figure 2-4a). The simulation shows an initial increase in membrane phosphoinositides at both sites of stimulation (Figure 2-4b). However, as time progresses only one phosphoinositide peak persists, and it is at the site of the stronger source,  $S_2$ . At the site of the weaker source,  $S_1$ , the initial buildup of phosphoinositides is completely extinguished.

The practical implication of this result is the following. In reality, it is unlikely that a cell will encounter two perfectly identical chemoattractant sources. The model therefore implies that regardless of the chemoattractant stimulus, the cell decides to migrate in one and only one direction.

In terms of the model, this property of unique localization can be explained as follows. Exposure to two unequal sources results in an initial surge of phosphoinositide synthesis at both sites of stimulation. However, since the source at  $S_2$  is stronger, phosphoinositide synthesis at  $S_2$  is larger than phosphoinositide synthesis at  $S_1$ . At the same time, there is more synthesis and diffusion of the inositol phosphates ( $I$ ) from  $\xi_2$  towards  $\xi_1$ . The net effect of  $I$ 's fast diffusion towards  $\xi_1$  is to increase the threshold at  $\xi_1$  and thus prevent peak formation.

This model exhibits unique localization for the parameter values chosen in Table 2-1. However, this property depends on the parameter values associated with the reaction and diffusion of the activator and the inhibitor. Variations in these parameter values can yield multiple localizations.

#### **The quasisteady state as a function of the chemoattractant stimulus**

More insight into the model can be gained by determining the properties of the quasisteady states corresponding to various chemoattractant profiles. Figure 2-5a shows three chemoattractant profiles with the same mean value ( $\lambda_m = 0.26$ ) but very different slopes. Figure 2-5b shows the bifurcation curves corresponding to these chemoattractant profiles. The bifurcation curves were obtained by varying the mean value,  $\lambda_m$ , of the

chemoattractant profiles. Thus, they reflect the quasisteady states obtained when the chemoattractant profiles are “lifted” vertically without undergoing any change of shape.

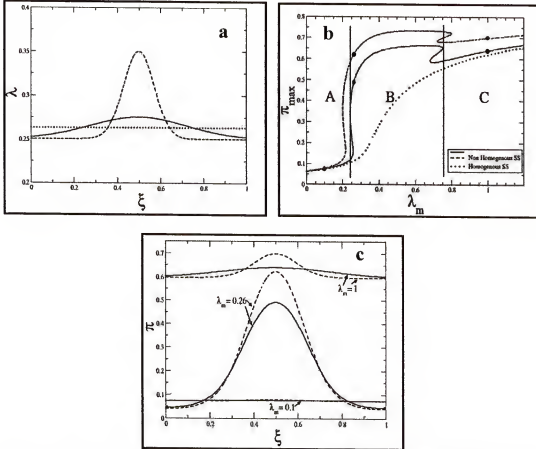


Figure 2-5. Variation of the quasi-steady state as a function of chemoattractant stimulus. (a) Three chemoattractant profiles with the same mean value but different gradients. (b) Variation of the maximum value of the corresponding quasisteady state phosphoinositide distributions with respect to the mean value of the chemoattractant profiles. (c) The quasisteady state phosphoinositide distributions corresponding to three different mean values. If the mean value lies in Regions A or C, the phosphoinositide distribution is nearly flat. If the mean value lies in Region B, the phosphoinositide distribution is strongly polarized.

We begin by examining the bifurcation curve corresponding to the uniform chemoattractant distribution (Figure 2-5b, dotted curve). Such uniform distributions result in homogeneous quasisteady states that satisfy equations (2.15–2.20) with  $\lambda = \lambda_m$ ,

$\mathcal{G}^- = 0$  and  $\delta_p = \delta_{p_s} = \delta_i = 0$ . The quasisteady state phosphoinositide concentration increases gradually, and then saturates at sufficiently large values of  $\lambda_m$ .

Next, consider the quasisteady states corresponding to the nonuniform chemoattractant distributions. The curves in Figure 2-5b and c show that when the mean values of the nonuniform chemoattractant distributions are small or large, both the maximum and the distribution of the quasisteady state phosphoinositide concentration become very similar to those observed in response to uniform chemoattractant distributions. However, there is an intermediate range of mean values over which the maxima and the distribution of the phosphoinositide concentration diverge dramatically from their homogeneous counterparts. For mean values lying within this intermediate range, the nonhomogenous quasisteady state phosphoinositide distributions are highly nonuniform.

These results can be rationalized as follows. As  $\lambda_m$  increases, so does the parameter,  $\kappa_f \mu$ , which is the ratio of the characteristic velocities of phosphoinositide synthesis and removal. If  $\lambda_m$ , and hence,  $\kappa_f \mu$  is small, the inhibitory action of the inositol phosphates is so fast compared to phosphoinositide synthesis that the phosphoinositide peak is abolished before it can form. If  $\lambda_m$  is large, the inositol phosphate pool responds so slowly compared to phosphoinositide synthesis that the peak spreads across the entire cell before the inhibition can contain it. In either case, the quasisteady state phosphoinositide distribution is nearly uniform. It is only at intermediate values of  $\lambda_m$  that the time scales of phosphoinositide synthesis and

inhibition are comparable, and nonuniform phosphoinositide distributions can be sustained.

### Polarized sensitivity

The model has also been used to explore the phenomenon of polarized sensitivity. To this end, a resting cell is allowed to form a quasisteady state phosphoinositide peak in response to a chemoattractant gradient,  $\lambda_1(\xi)$ . This quasisteady state is the initial condition of the cell. Thus,  $\mathcal{G}^- = 0$  and  $\pi^-, \pi_s^-, i^-$  satisfy the boundary value problem defined by the equations

$$\begin{aligned}\mu &= \frac{\lambda_1}{1 + \lambda_1} - \mathcal{G}^- \\ 0 &= \kappa_f \mu \pi^2 \pi_s - \pi i + \psi_p - \kappa_p \pi + \delta_p \frac{\partial^2 \pi}{\partial \xi^2} \\ 0 &= -\left( \kappa_f \mu \pi^2 \pi_s - \pi i + \psi_p - \kappa_p \pi \right) + \delta_p \frac{\partial^2 \pi_s}{\partial \xi^2} \\ 0 &= \kappa_f \mu \pi^2 \pi_s - \pi i + \psi_i - \kappa_i i + \delta_i \frac{\partial^2 i}{\partial \xi^2}\end{aligned}$$

and the boundary conditions (2.19). After the quasi-steady state is reached, the polarized cell is subjected to a new chemoattractant gradient,  $\lambda_2(\xi) \neq \lambda_1(\xi)$ . The subsequent evolution of  $P$ ,  $P_s$  and  $I$  in response to this new gradient is obtained by integrating (2.15–2.20) with  $\lambda = \lambda_2(\xi)$ .

The simulations show that if the new chemoattractant gradient declines gradually from its maximum in such a way that the receptors in the neighborhood of the pre-existing phosphoinositide peak sense the influence of the new gradient, the pre-existing peak moves like a traveling wave to the point at which the new chemoattractant gradient

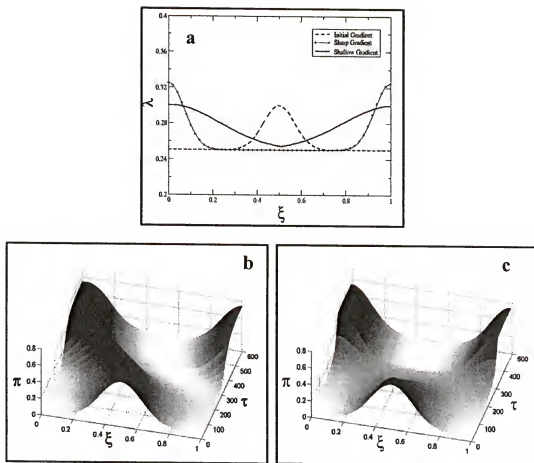


Figure 2-6. Response of a pre-existing phosphoinositide peak to a new gradient. (a) The active receptor concentration (b) When the new gradient is shallow, the phosphoinositide peak moves as a traveling wave towards the new steady state (c) If the new gradient is localized and large enough, the original phosphoinositide peak collapses and a new peak is created at the maximum of the new gradient.

has a maximum (Figure 2-6b). On the other hand, if the new chemoattractant profile is large enough to overcome the threshold and is localized such that the pre-existing leading edge does not sense the new gradient, then there is no wave motion. Instead, the pre-existing peak retracts, and a new peak grows at the maximum of the new gradient (Figure 2-6c). These results are consistent with the phosphoinositide dynamics observed in response to changes in chemoattractant gradients.

To explain the wave-like motion of the peak shown in Figure 2-6b, it is useful to observe that the quasi-steady phosphoinositide peak formed in response to the first gradient is “inert” everywhere except in the two thin “transition layers” surrounding the peak within which there is a sharp change in the gradient of membrane phosphoinositides. By “Inert”, it means that outside these transition layers, nothing is happening at steady state - there is neither diffusion nor synthesis of membrane phosphoinositides. The transition layers, on the other hand, are sites of intense activity. In the upper half of a transition layers, there is rapid synthesis of membrane phosphoinositides which then diffuse into the lower half of the transition layer, from where they are promptly removed. The quasi-steady state is maintained by this precarious balance between synthesis of membrane phosphoinositides in the upper half of the transition layers and their removal in the lower half of the transition layers. If the balance is disturbed by imposing a shallow chemoattractant gradient that increases the rate of phosphoinositide synthesis relative to its rate of diffusion, the transition layer moves in a wave-like fashion at a velocity that is proportional to the net rate of phosphoinositide accumulation within the transition layer.

The response to steep chemoattractant gradients shown in Figure 2-6c can be explained as follows. After the quasi-steady state has developed, the concentration of the inhibitor,  $I$ , is high throughout the cell. This tends to increase the threshold at all points of the plasma membrane. When the gradient is switched, the active receptor concentration decreases at the previous “front” and increases at the current “front”. It follows from the earlier discussion regarding thresholds that at the current “front”, there

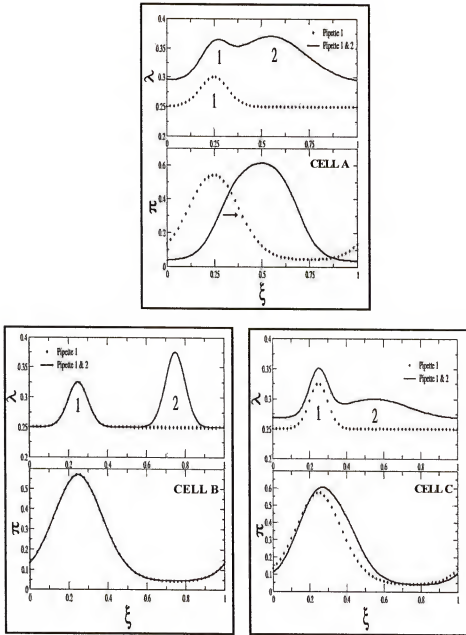


Figure 2-7. Simulation of data in shown in Figure 1-6. Top: The chemoattractant profiles for cells *a*, *b*, and *c*, respectively. Bottom: The dotted lines show the quasisteady state profiles attained in response to pipette 1. The full lines show the new quasisteady state profiles attained in response to pipettes 1 and 2. Cell *a* responds to the new chemoattractant source by translocating the phosphoinositide peak in a wave-like motion. Cells *b* and *c* are essentially unaffected by the new chemoattractant source.



is a tendency for the threshold to increase due to elevated inhibitor concentrations. If the perturbation is large enough at the current “front”, this threshold is mitigated and a new peak forms. However, at the “previous” front, the tendency of the threshold to increase due to elevated inhibitor concentrations is further exacerbated by the lower active receptor concentration. The thresholds at the “previous” front become so large that despite the large concentrations of membrane phosphoinositides, they fall short of the threshold, and the pre-existing peak collapses.

Along the same lines, the experiment shown in Figure 1-7 can be simulated. The model cells are exposed to pipette 1 and are allowed to form quasi-steady phosphoinositide peaks consistent with the external gradients imposed on them (dotted lines in Figure 2-7). According to the model the closer the cell is to the pipette, the more intensely polarized it becomes (dotted lines, Fig 2-7). Subsequently, all three cells are exposed to an additional pipette 2 and allowed to reach a new quasisteady state (full lines in Figure 2-7). The results of the simulation are consistent with the experimental observations

- The leading edge of cell *a* senses a shallow gradient from pipette 2. However, since pipette 1 exerts a weak influence on this cell, the pre-existing peak is easily dislocated and moves like a traveling wave towards pipette 2 (Figure 2-7, Cell a).
- The trailing edge of cell *b* experiences the strong influence of pipette 2. But, the pre-existing influence of pipette 1 is so strong that the cell does not entertain the signal from pipette 2 (Figure 2-7, Cell b). To understand this, it suffices to note that the stronger the pre-existing polarity, the higher the concentration of the inhibitory pool of *I*. Hence, the strength of the signal required to provoke a new peak increases with the intensity of the pre-existing polarity.
- The leading edge of cell *c* senses only a weak gradient from pipette 2. In addition, since pipette 1 exerts a strong influence on cell *c*, the phosphoinositide peak remains unaffected (Figure 2-7c, Cell c).

## Slow Responses

To study the effect of adaptation on the phosphoinositide dynamics, the reduced model (2.7–2.14) should be considered.

## Adaptation

To simulate the effect of adaptation, imagine that a resting cell is suddenly exposed to a uniform chemoattractant concentration,  $\lambda^+$ . Since the environment is uniform, diffusion plays no role, and the evolution of the system is given by ODEs obtained when  $\delta_p = \delta_{p_s} = \delta_l = 0$  in equations (2.7–2.14).

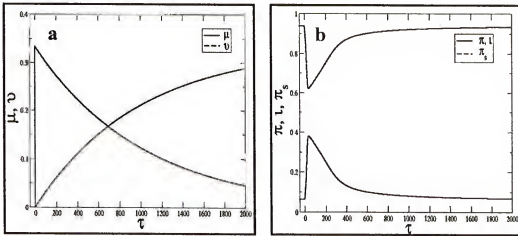


Figure 2-8. Adaptation in response to a uniform increase in the chemoattractant concentration. (a) Evolution of the adaptation subsystem. The fast variable,  $\mu$ , rapidly increases from zero to  $\lambda^+/(1 + \lambda^+)$ , but returns to zero as the slow variable,  $\varrho$ , gradually increases from zero to  $\lambda^+/(1 + \lambda^+)$ . (b) Evolution of the polarization subsystem. All three variables change rapidly on a fast time scale and return to their resting levels on a slow time scale.

Figure 2-8 shows the evolution of the model variables for  $\lambda^+ = 0.5$ . Consistent with the experiments,  $\mu$  and  $\pi$  increase on a time scale of 1 second. On a slow time scale of 1000 seconds,  $\varrho$  approaches  $\rho(\lambda^+)$  and  $\mu$  approaches zero, so that  $\pi$ ,  $\pi_s$  and  $l$  return to their resting values.

This simulation can be understood by appealing to Figure 2-8b. In the absence of diffusion, the non-uniform steady state does not exist and the uniform steady state is stable. The system therefore evolves along the locus of uniform steady states (dotted curve in Figure 2-8b). Initially,  $\pi$  jumps rapidly from its basal value to its maximum value. This rapid transient is followed by a slow decline along the path of uniform steady states.

### Spontaneous polarization

The above simulation of adaptation appears to contradict the experimental data. For, the simulations imply that the cells remain in a uniform steady state throughout the transient, but the experiments show that the cells frequently polarize before they adapt. This contradiction can be resolved by observing that single cells receive noisy signals. Indeed, the random location of the polarity in spontaneous polarization implies that some variable that is upstream of the phosphoinositides undergoes stochastic fluctuations. The most upstream source of stochastic fluctuations is the concentration of the chemoattractant. We show below that fluctuations of the chemoattractant concentration are sufficient to trigger spontaneous polarization of the cell.

To model the fluctuations, we assume that the uniformly distributed chemoattractant around the cell is in thermodynamic equilibrium. Then it follows from the theory of fluctuations [64] that the chemoattractant concentration has a Gaussian distribution with mean, say  $I_m$ , and variance  $(\kappa kT/V)^{1/2} I_m$ , where  $\kappa$  is the isothermal compressibility at temperature  $T$ ,  $k$  is Boltzmann's constant, and  $V$  is the characteristic volume of chemoattractant sampled by the receptors. A reasonable approximation for the

extracellular sample volume,  $V$ , is  $(D_l/k^-)^{3/2}$  where  $D_l$  is the diffusion coefficient of the chemoattractant, and  $k^-$  is the dissociation rate constant for receptor-ligand binding [65].

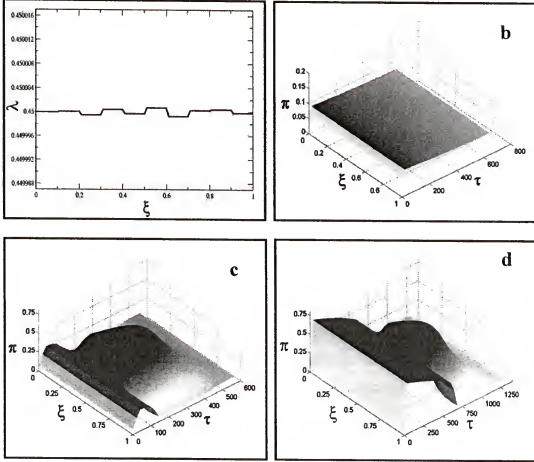


Figure 2-9. Spontaneous polarization in response to a uniform but noisy chemoattractant profile. Parameter values used:  $n = 10$ ,  $T = 298$  K,  $\kappa = 45 \times 10^{-11}$  1/Pa,  $D_l = 10^{-10}$  m<sup>2</sup>/s. (a) Snapshot of the noisy chemoattractant profile generated by the stochastic model. (b) Uniform increase and return to rest state without any spontaneous polarization. Observed for  $\lambda^* = 0.2$ . (c) Uniform increase followed by the formation and disruption of a phosphoinositide peak. Observed for  $\lambda^* = 0.45$ . (d) Uniform increase and decrease of phosphoinositides, followed by peak formation and disruption. Observed for  $\lambda^* = 1.5$ .

If we partition the sample volume ( $V$ ) into  $n$  equal sections, the evolution of the ligand concentration in each section is given by the stochastic equation

$$l_i(t) = l_m(1 + \sqrt{\frac{\kappa k T}{V_i}} z_i), i = 1, 2, \dots, n \quad (2.22)$$

where  $V_i$  is the volume of each section,  $V/n$  and  $z_i$  is a Gaussian random number generator with zero mean and unit variance. Introducing the dimensionless quantities  $\lambda \equiv l/(k^+/k^-)$  and  $\phi_i \equiv (\kappa k T/V_i)^{1/2}$ , we may rewrite equation (2.22) as

$$\lambda_i(\tau) = \lambda_m(1 + \phi_i z_i), i = 1, 2, \dots, n \quad (2.23)$$

To simulate the experiments showing spontaneous polarization, it is assumed that at  $\tau < 0$ , the cell is exposed to a small and uniform chemoattractant concentration,  $\lambda_m = \lambda^-$ . At  $\tau \geq 0$ , the cell is immersed in a mean concentration,  $\lambda^+ > \lambda^-$ . Sampling the random number generator ( $z_i$ ) for each section independently, at every  $d\tau = 0.01$ , equation (2.23) yields a noisy active ligand distribution. A typical snapshot of this distribution is shown in Figure 2-9a. The response to the noisy ligand concentration is then simulated by introducing  $\lambda(\tau, \xi)$  in the model equations (2.7-2.14).

Depending on the magnitude of  $\lambda^+$ , three types of responses are obtained (Figure 2-9b, c, d). These responses are consistent with the experimental observations of [66]. To understand these responses, observe that the noise in the ligand concentration induces minute gradients. Beyond a critical  $\lambda_{m, \text{mean}}^+$ , this non-uniform environment, makes the rest state unstable in the Turing sense, i.e., stable to homogenous perturbations and unstable to the smallest non-homogeneity [67]. Hence, as the system adapts, it evolves along the path of nonuniform steady states on the bifurcation diagram (Figure 2-5b). Thus

1. If  $\lambda^+$  is small,  $\pi$  increases uniformly and then returns to its rest state without any spontaneous polarization during the transient (Figure 2-9b).

2. At intermediate values of  $\lambda^+$ ,  $\pi$  increases uniformly on a fast time scale, but then breaks out into a nonuniform distribution. As time evolves, the width of the peak progressively decreases until the peak disappears completely and the system returns to its rest state (Figure 2-9c).
3. If  $\lambda^+$  is large,  $\pi$  increases uniformly on a fast time scale, and then decreases uniformly on a slow time scale before erupting into a nonuniform distribution. The polarization gradually decreases and the system returns to its rest state (Figure 2-9d).

Here, adaptation of variable  $\mu$  brings the system back to its rest state and causes disruption of the peak.

These results are consistent with the sensory adaptation observed in human neutrophils [29]. The time taken for the rapid uniform increase is relatively independent of the chemoattractant concentration. On the other hand, the time taken for the spontaneous polarization to occur increases with the mean chemoattractant concentration.

### CHAPTER 3 MATHEMATICAL ANALYSIS

Since the molecular basis of gradient sensing is not completely known, it seems premature to expect quantitative answers from the mathematical model. However, one can still appeal to the mathematical model for answers concerning qualitative properties. For example, it is quite relevant to ask: What are the factors that determine the geometry of the phosphoinositide localization? What are the conditions that allow for the formation of the phosphoinositide localization from a homogenous resting state? Such questions can be answered by a mathematical analysis of the model.

The polarization subsystem of the model is a boundary value problem with periodic boundary conditions and the phosphoinositide localization is a non-uniform steady state solution of this problem. Since the diffusivity of membrane phospholipids is three orders of magnitude smaller than the diffusivity of the cytosolic pool of inositol phosphates, the boundary value problem contains a small parameter, namely the ratio of the two diffusivities. Approximations to the non-uniform steady states can therefore, be obtained by appealing to a technique called singular perturbation theory. This approach, originally developed by [68], has been successful for analyzing activator-inhibitor models in which the inhibitor diffuses much more rapidly than the activator. The first half of this chapter describes this approach for the analytical construction of the phosphoinositide steady state. It will allow us to obtain approximate geometrical properties of the phosphoinositide steady state such as width and height. We shall also use this study to understand how variation in phosphoinositide synthesis can lead to change in peak width.

The second half of this chapter deals with a stability analysis for the homogenous phosphoinositide resting state. This analysis provides insight into the range of phosphoinositide synthesis rates that cause the homogenous resting state, to lose stability and spontaneously polarize into a phosphoinositide localization.

### Simplified Polarization Subsystem

It has been experimentally shown that the addition of extracellular membrane permeant  $\text{PIP}_3$  to resting cells can initiate spontaneous polarization of intracellular phosphoinositides, morphological polarity and motility, in the absence of any added chemoattractant. This suggests that the polarization subsystem can be stimulated independent of receptor activation and the adaptation subsystem.

This experiment can be modeled by perturbing the intracellular concentration of phosphoinositides and studying the response of the polarization subsystem. The model can be further simplified by assuming that the sum of phosphoinositide concentrations in the membrane and endoplasmic reticulum is a constant ( $p_i \equiv p + p_s \approx \text{constant}$ ), over the time scale of the experiment. This assumption reduces the polarization subsystem to the following equations,

$$\frac{\partial p}{\partial t} = k_f p^2 (p_i - p) - k_r p i + c_p - k_p p + \frac{D_p}{R^2} \frac{\partial^2 p}{\partial \theta^2} \quad (3.1)$$

$$\frac{\partial i}{\partial t} = s \{ k_f p^2 (p_i - p) - k_r p i \} + c_i - k_i i + \frac{D_i}{R^2} \frac{\partial^2 i}{\partial \theta^2} \quad (3.2)$$

with periodic boundary conditions,

$$x(0, \tau) = x(1, \tau), \frac{\partial x(0, \tau)}{\partial \xi} = \frac{\partial x(1, \tau)}{\partial \xi}, \tau > 0 \quad (3.3)$$

$$x = p, i$$

and initial conditions



$$\overline{p}(\theta, 0) = p^-(\theta), \quad i(\theta, 0) = i^-(\theta), \quad 0 \leq \theta < 2\pi \quad (3.4)$$

where  $p^-(\theta)$  and  $i^-(\theta)$  are chosen to reflect the perturbation imposed in the experiment.

Using the dimensionless variables

$$\pi \equiv \frac{p}{p_i}, \quad t \equiv \frac{i}{sp_i}, \quad \xi \equiv \frac{\theta}{2 \times 3.1416}, \quad \tau \equiv \frac{t}{l/(k_r sp_i)}$$

and dimensionless parameters

$$\begin{aligned} \delta_p &\equiv \frac{D_p \kappa^2}{k_r sp_i} & \psi_p &\equiv \frac{c_p p_i}{k_r sp_i} & \kappa_p &\equiv \frac{k_p}{k_r sp_i} & \kappa_f &\equiv \frac{k_f p_i^2}{k_r sp_i} \\ \delta_i &\equiv \frac{D_i \kappa^2}{k_r sp_i} & \psi_i &\equiv \frac{c_i p_i}{k_r sp_i} & \kappa_i &\equiv \frac{k_i}{k_r sp_i} \end{aligned}$$

equations (3.1)–(3.4) can be rewritten as

$$\frac{\partial \pi}{\partial \tau} = \kappa_f \pi^2 (1 - \pi) - \pi t + \psi_p - \kappa_p \pi + \delta_p \frac{\partial^2 \pi}{\partial \xi^2} \quad (3.5)$$

$$\frac{\partial t}{\partial \tau} = \kappa_f \pi^2 (1 - \pi) - \pi t + \psi_i - \kappa_i t + \delta_i \frac{\partial^2 t}{\partial \xi^2} \quad (3.6)$$

with dimensionless boundary conditions

$$\begin{aligned} x(0, \tau) = x(1, \tau), \quad \frac{\partial x(0, \tau)}{\partial \xi} = \frac{\partial x(1, \tau)}{\partial \xi}, \quad \tau > 0 \\ x \equiv \pi, t \end{aligned} \quad (3.7)$$

and dimensionless initial conditions.

$$\pi(0, \xi) = \pi^-, \quad t(0, \xi) = i^-, \quad 0 \leq \xi < 1 \quad (3.8)$$

$\kappa_f = 1.5$  has been used for the following simulation. All other parameter values are the

same as in Table 2-1. Before the phosphoinositide perturbation is applied ( $\tau < 0$ ),  $P$  and

$I$  are in a homogeneous steady state  $(\bar{\pi}, \bar{t})$ , determined by the equations

$$\kappa_f \bar{\pi}^2 (1 - \bar{\pi}) - \bar{\pi} \bar{t} + \psi_p - \kappa_p \bar{\pi} = 0$$

$$\kappa_f \bar{\pi}^2 (1 - \bar{\pi}) - \bar{\pi} \bar{t} + \psi_i - \kappa_i \bar{t} = 0$$

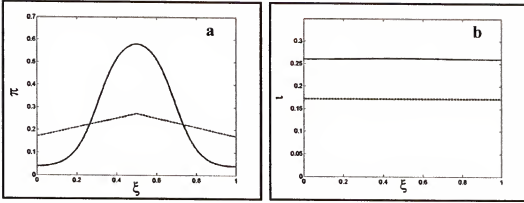


Figure 3-1. Steady states of the reduced model. Dashed lines denote initial conditions; Solid lines denote steady state response. (a) Phosphoinositides  $\pi(\xi)$  (b) Inositol phosphates  $\iota(\xi)$ .

At  $\tau = 0$ , the homogenous steady state of the phosphoinositides ( $\bar{\pi}$ ) is subjected to a non-uniform perturbation ( $\pi = \bar{\pi} + \Delta\pi(\xi)$ ) such that concentration is highest at the leading edge ( $\xi = 1/2$ ) and lowest at the trailing edge ( $\xi = 0, 1$ ). A pronounced phosphoinositide peak develops at the leading edge ( $\xi = 1/2$ ) (Figure 3-1a). Compared to the polarized distribution of membrane phosphoinositides, the concentration profile of inositol phosphates is essentially flat (Figure 3-1b). All the analysis performed in the following sections will be based on this simplified model.

### Evolution of the Phosphoinositide Localization

The evolution of the phosphoinositide localization is a two-fold process. Firstly, if a certain threshold is crossed, membrane phosphoinositides develop large spatial gradients from their homogenous initial state. This evolution reaches a state of quasi equilibrium rapidly. In the second phase, the large gradients that form move outward on a slow time scale, until a steady state is reached.

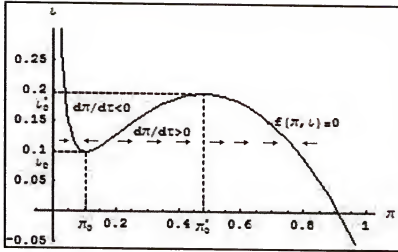


Figure 3-2. Nullcline  $d\pi/d\tau = f(\pi, \iota) = 0$ . All points above the curve ( $d\pi/d\tau < 0$ ) move towards lower  $\pi$  and all points below the curve ( $d\pi/d\tau > 0$ ) move towards higher  $\pi$ .

### First Phase

Since the spatial gradients in  $P$  are initially small, diffusion can be neglected and the *initial* evolution of  $P$  can be approximated by

$$\begin{aligned} \frac{\partial \pi}{\partial \tau} &= \kappa_f \pi^2 (1 - \pi) - \pi \tilde{\iota} + \psi_p - \kappa_p \pi = -f(\pi, \iota) \\ \pi(\xi, 0) &= \pi^- = \tilde{\pi} + \Delta\pi(\xi) \end{aligned} \quad (3.9)$$

where  $\pi(\xi, 0)$  denotes the initial distribution of  $P$ . During this period, it is assumed that the concentration of  $\iota$  is held fixed at its initial value  $\iota^- = \tilde{\iota}$ . If  $\pi$  at the leading edge of the cell crosses the threshold for amplification, i.e. if the perturbation is in the region where  $\frac{d\pi}{d\tau} > 0$ , the initial point immediately increases towards higher  $\pi$  (see Figure 3-2).

In contrast, if the trailing edge of the cell does not feel the perturbation,  $\pi$  will lie below the threshold for amplification (the region where  $\frac{d\pi}{d\tau} \leq 0$ , see Figure 3-2), forcing  $\pi$  to either decrease or stay at  $\pi = \pi^-$ .

Since, the phosphoinositides in the membrane either reach a high steady state or a low steady state, the first phase of evolution results in a state of quasi-equilibria – two smooth, distinct subregions separated by sharp transition layers.

### Second Phase

At the end of the first phase, each of the subregions reaches a steady state. However, the sharp transition layers between these subregions are in a state of imbalance, since there is more synthesis of phosphoinositides than removal. The imbalance in phosphoinositides causes the walls of the transition layers to move outward like a traveling wave, until there is no more accumulation of phosphoinositides within the transition layer. This eventually results in the formation of the steady state, phosphoinositide localization.

### Construction of the Non-homogenous Steady State

The non-homogenous steady state of the model satisfies

$$\delta_p \frac{d^2 \pi}{d\xi^2} = f(\pi, t) = -\kappa_f \pi^2 (1 - \pi) + \pi t - \psi_p + \kappa_p \pi \quad (3.10)$$

$$\delta_i \frac{d^2 t}{d\xi^2} = g(\pi, t) = -\kappa_f \pi^2 (1 - \pi) + \pi t - \psi_i + \kappa_i \pi \quad (3.11)$$

with periodic boundary conditions  $\mu(0) = \mu(1)$  and  $\frac{d\mu}{d\xi}(0) = \frac{d\mu}{d\xi}(1)$ , where  $\mu = \pi, t$ .

Here  $f(\pi, t)$  denotes the rate of removal of membrane phosphoinositides ( $P$ ) and  $g(\pi, t)$  the rate of removal of cytosolic inositol phosphates ( $I$ ).

As discussed earlier, it is important to note that a stable non-homogenous steady state in  $\pi$  can form only when  $\delta_p \ll \delta_i$ . Problems of this type where a small parameter  $\delta_p$  multiplies the highest derivative usually give rise to singular solutions, that undergo

rapid transitions in  $\xi$  [69]. In these cases, it becomes difficult to find a complete analytical solution that is valid for all  $0 < \xi < 1$ . The standard way to tackle this difficulty is to seek a solution which ignores diffusion in  $\pi$  everywhere except for the region where  $\pi$  changes sharply. In other words, it is assumed that the solution comprises of two regions: (1) An 'outer' solution where  $\pi$  changes slowly with  $\xi$  and diffusion can be neglected (2) An 'inner' solution where  $\pi$  changes fast with  $\xi$  and diffusion needs to be taken into account. The outer solution will yield smooth subregions that are separated by discontinuities, which arise because diffusion of  $P$  has been ignored. The inner solution corresponds to the sharp interface that should exist at these points of discontinuities. On patching up these two solutions, an approximate steady state peak can be constructed [67, 70, 71].

### Outer Solution

First, assume that the diffusion of  $\pi$  is small everywhere (i.e.  $\delta_p \frac{d^2 \pi}{d\xi^2} \approx 0$ ). Setting  $\delta_i = 1$  and using regular perturbation expansions in small parameter  $\delta_p$ ,  $\pi \equiv \pi^{(0)} + \delta_p \pi^{(1)} \dots$  and  $t \equiv t^{(0)} + \delta_p t^{(1)} \dots$ , the zeroth order equations ( $\delta_p = 0$ ) for (3.10) and (3.11) can be written as

$$f(\pi, t) = -\kappa_f \pi^2 (1 - \pi) + \pi t - \psi_p + \kappa_p \pi = 0 \quad (3.12)$$

$$\frac{d^2 t}{d\xi^2} = g(\pi, t) = -\kappa_f \pi^2 (1 - \pi) + \pi t - \psi_i + \kappa_r \pi \quad (3.13)$$

The function  $f(\pi, t) = -\kappa_f \pi^2 (1 - \pi) + \pi t - \psi_p + \kappa_p \pi = 0$  is an S-shaped curve that has a maximum in  $t$  at  $(\pi_0', t_0')$  and a minimum at  $(\pi_0, t_0)$  (Figure 3-2, 3-4a).

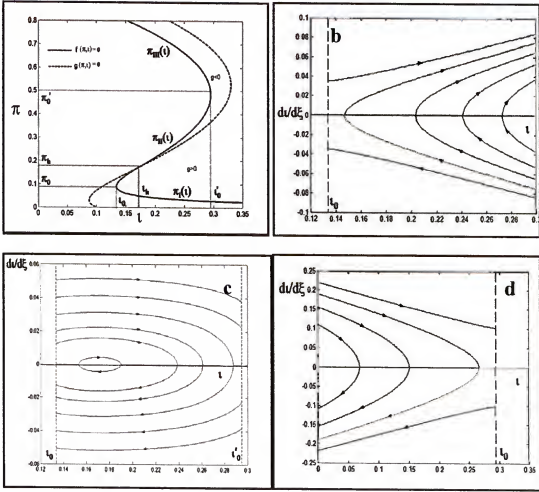


Figure 3-4. Phase portraits for each branch of  $f(\pi, t) = 0$  (a) Nullclines  $f(\pi, t) = 0$  and  $g(\pi, t) = 0$ . For,  $\kappa_f = 1.5$ ,  $g(\pi, t) = 0$  intersects the lower branch of  $f(\pi, t) = 0$  at  $(\pi_h, t_h)$  (b) Phase portrait for lower branch I (c) Phase portrait for middle branch II (d) Phase portrait for upper branch III

The nullcline  $f(\pi, t) = 0$  has three separate roots

$$\pi(t) = \begin{cases} \pi_l(t) & \text{If } \pi < \pi_0 - \text{Lower Branch I} \\ \pi_m(t) & \text{If } \pi_0 < \pi < \pi_0' - \text{Middle Branch II} \\ \pi_u(t) & \text{If } \pi > \pi_0' - \text{Upper Branch III} \end{cases} \quad (3.14)$$

Using the roots of  $f(\pi, t) = 0$ , equation (3.13) can be reduced to

$$\frac{d^2 \iota}{d\xi^2} = g(\pi_j(\iota), \iota) \quad \text{where } j = \text{I, II, III} \quad (3.15)$$

with periodic boundary conditions  $\iota(0) = \iota(1)$  and  $\frac{d\iota}{d\xi}(0) = \frac{d\iota}{d\xi}(1)$ . Since the diffusion of  $I$  is fast, only continuous solutions for  $\iota(\xi)$  are expected. In order to solve for the outer solution,  $\iota(\xi)$ , the equation (3.15) can be rewritten in the form of a conservative system,

$$\frac{d\iota}{d\xi} = \pm \sqrt{2(E - \phi_\iota)} \quad (3.16)$$

where  $\phi_\iota$  denotes the potential of the system and  $E(\iota, \iota'_\xi)$  is the Hamiltonian.

Equation (3.16) can be used to draw the phase plane (Figure 3-4), for each branch of  $\pi(\iota)$ . Any orbit that starts from a point on the phase plane (at  $\xi = 0$ ) and returns to the very same point within  $\xi = 1$  would be a valid solution of (3.15) and would satisfy the periodic boundary conditions.

Branch II can yield valid solutions to the problem (3.15) (Figure 3-4c). However, solutions arising from this branch turn out to be unstable, and therefore have to be dismissed [67]. From inspecting the orbits of branch I and branch III (Figure 3-4 b, d), one can conclude that none of these orbits satisfy periodic boundary conditions – since none of the orbits close.

Closer examination of these phase portraits reveals another possibility: A solution with the required period (see figure 3-5, orbit ABCB'A) can be constructed by patching together orbits of branch III with the orbits of branch I. Since, every point on this unique orbit can be chosen as a starting point ( $\xi = 0$ ), infinite such solutions are possible. These solutions are just lateral translations of one another in space.

For specificity, let us restrict ourselves to constructing a solution that has one maxima ( $n=1$ ) at  $\xi = 1/2$ . Solutions with more than one maxima ( $n>1$ ) can also be constructed (see  $n=2$ , Figure 3-5). However, these solutions turn out to be unstable [67].

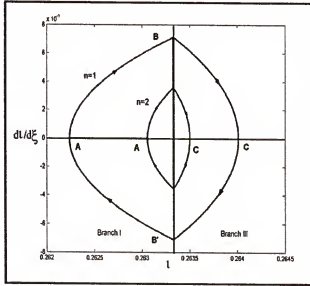


Figure 3-5. Patched phase plane for the outer solution  $\iota(\xi)$ . The outer orbit  $ABCB'A$  is a solution with a single maximum in  $\iota(\xi)$  ( $n=1$ ). The inner orbit  $AC$  is a solution that has two maxima in  $\iota(\xi)$  ( $n=2$ ).

In order to construct the ( $n=1$ ) solution ( $ABCB'A$ ), assume an arbitrary point,  $\iota_0 < \iota^* < \iota'_0$ , for patching up branch I and branch III. Consider an orbit that starts at a point  $A(\alpha, 0)$  (with  $\alpha > \iota_0$ ) on the branch I phase plane (see Figure 3-5) and follow the orbit to a point  $B(\iota^*, \iota'_2)$ . Transfer this point to the branch III phase plane, and follow the corresponding orbit. If this orbit reaches point  $C(\beta, 0)$  in  $\xi = 1/2$ , the orbit would satisfy (3.15) and its boundary conditions. Note that only a specific choice of  $\alpha$  will pick up the desired solution. This particular  $\alpha$  can be found by imposing (i) continuity of the patched solution at  $\iota = \iota^*$  and the (ii) size of the system ( $\Delta\xi = 1$ ).



In order to patch up the orbits, let us define the Hamiltonian of a particular orbit as

$$E^{(I,III)}(t, t'_\epsilon) = \frac{1}{2} (t'_\epsilon)^{(I,III)}{}^2 + \phi_t^{(I,III)} \quad (3.17)$$

where the potential  $\phi_t^{(I,III)} = -\int^t g(\pi_{I,III}(t), t) dt$ .

The solution to (3.15) must satisfy the following conditions.

1. Continuity at  $t = t^*$ : In order to ensure the continuous transition of the branch I solution to branch III and vice versa (at  $B$  and  $B'$ , Figure 3-5a) the following conditions have to hold,

$$t'_\epsilon \Big|_B^{(I)} = t'_\epsilon \Big|_B^{(III)} = t'_\epsilon \quad (3.18)$$

$$t'_\epsilon \Big|_{B'}^{(I)} = t'_\epsilon \Big|_{B'}^{(III)} = -t'_\epsilon \quad (3.19)$$

$$t_{B,B'}^{(I)} = t_{B,B'}^{(III)} = t^* \quad (3.20)$$

Using (3.17), (3.20) and the fact that the Hamiltonian of a particular orbit is constant, the following condition should hold for branch I

$$E^{(I)}(t, t'_\epsilon) = E_A^{(I)}(\alpha, 0) = E_{B,B'}^{(I)} \quad (3.21)$$

$$\Rightarrow \phi_\alpha^{(I)} = \frac{1}{2} (t'_\epsilon \Big|_{B,B'}^{(I)})^2 + \phi_t^{(I)} \quad (3.22)$$

Similarly, for branch III

$$E^{(III)}(t, t'_\epsilon) = E_c^{(III)}(\beta, 0) = E_{B,B'}^{(III)} \quad (3.23)$$

$$\Rightarrow \phi_\beta^{(III)} = \frac{1}{2} (t'_\epsilon \Big|_{B,B'}^{(III)})^2 + \phi_t^{(III)} \quad (3.24)$$

Using (3.18), (3.19), (3.22) and (3.24) the following condition can be written

$$\int_\alpha^\alpha g(\pi_I(t), t) dt = \int_\beta^\beta g(\pi_{III}(t), t) dt \quad (3.25)$$

2. Periodic Boundary Conditions at  $\xi = 0, 1$ : The time taken for moving through the orbit ABCB'A should be equal to the width of the system ( $\Delta\xi = 1$ ). This can be used to derive a time-map equation. Rearranging (3.17) for branches I and III, and using (3.21), (3.23) we have

$$|t_\xi^{(I,III)}| = \sqrt{2 \int_{\alpha, \beta} g(\pi_{i,m}(t), t) dt} \quad (3.26)$$

Using (3.26) the following equations can be written

$$\begin{aligned} A \rightarrow B: \int_0^{\xi_B} &= \int_\alpha^{\xi^*} \frac{dt}{\sqrt{2 \int_\alpha^t g_i dt}}; & B \rightarrow C: \int_{\xi_B}^{\xi_{B'}} &= \int_{\xi^*}^\beta \frac{dt}{\sqrt{2 \int_\beta^t g_m dt}} \\ C \rightarrow B': \int_{\xi_{B'}}^{\xi^*} &= \int_\beta^{\xi^*} \frac{-dt}{\sqrt{2 \int_\beta^t g_m dt}}; & B' \rightarrow A: \int_{\xi^*}^0 &= \int_{\xi^*}^\alpha \frac{-dt}{\sqrt{2 \int_\alpha^t g_i dt}} \end{aligned} \quad (3.27)$$

Here,  $\xi_B$  and  $\xi_{B'}$  denote the  $\xi$  values at points B and B'. Adding these four

integrals, the following time-map condition can be written

$$\Delta\xi = 1 = \sqrt{2} \left[ \int_\alpha^{\xi^*} \frac{dt}{\sqrt{\int_\alpha^t g_i dt}} + \int_{\xi^*}^\beta \frac{dt}{\sqrt{\int_\beta^t g_m dt}} \right] \quad (3.28)$$

For a given  $t = t^*$ ,  $\alpha$  and  $\beta$  can be found by solving conditions (3.25) and (3.28)

simultaneously. Knowing  $\alpha$  and  $\beta$ , the unknowns  $\xi_B, \xi_{B'}, t_\xi^*$  can be found using

equations (3.22) and (3.27). The unknown patching point,  $t = t^*$  can be determined

from a continuity condition for the inner and outer solution of the problem. This

will be discussed in the following section. Assuming  $t^*$  is known, the following

equations can be numerically solved for the outer solution  $t(\xi)$ ,

$$\frac{d^2 t^{(j)}}{d\xi^2} = g(\pi(t^{(j)}), t^{(j)}) \quad (3.29)$$

$$f(\pi_j, t^{(j)}) = 0 \Rightarrow \pi = \pi_j(t^{(j)}) \quad j = I, III \quad (3.30)$$

using (i) Periodic boundary conditions on  $\iota^{(I)}(\xi)$  at  $\xi = 0, 1$ ,  $\iota^{(III)}(1/2) = \beta$  and  $\iota_\xi^{(III)}(1/2) = 0$  (ii) Continuity conditions (3.18), (3.19) and (3.20). Although  $\iota$  is continuous at  $\xi = \xi_{B,B'}$ , the corresponding solution for  $\pi(\xi)$  (from (3.30)) has a discontinuous transition from branch I to branch III or vice versa (see Figure 3-6), i.e.,

$$\begin{aligned}\pi(\xi_{-B}) &= \pi(\xi_{+B}) \approx \pi_I(\iota^*) \\ \pi(\xi_{+B}) &= \pi(\xi_{-B}) \approx \pi_{III}(\iota^*)\end{aligned}\tag{3.31}$$

Here,  $\xi \pm_{B,B'}$  refers to a small displacement on either side of  $\xi = \xi_{B,B'}$ .

Hence, the outer solution,  $\pi(\xi)$  (Figure 3-6), consists of two distinct subregions, a low steady state  $\pi_I(\iota(\xi))$  and a high steady state  $\pi_{III}(\iota(\xi))$ . As expected, each of these subregions is separated by discontinuities at points of patching  $\xi = \xi_{B,B'}$ . The concentration of  $\pi$  in each of these subregions alters itself according to the local concentration of  $\iota$ , such that there is no net formation of membrane phosphoinositides ( $f(\pi, \iota) = 0$ ).

The above calculations also allow us to evaluate approximate geometrical properties of the phosphoinositide localization, such as width of the localization,  $\xi_B - \xi_{B'}$  and height of the localization,  $\pi_{III}(\iota(\xi_{B,B'})) - \pi_I(\iota(\xi_{B,B'}))$ .

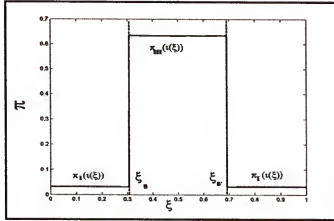


Figure 3-6. Outer solution  $\pi(\xi)$ . Discontinuities exist at  $\xi_B$  and  $\xi_{B'}$ . Solution between  $\xi_B$  and  $\xi_{B'}$  corresponds to  $\pi_{III}(u(\xi))$ . Solution to the left of  $\xi_B$  and to the right of  $\xi_{B'}$ , corresponds to  $\pi_I(u(\xi))$ .

Therefore, at the end of the first stage of evolution, the phosphoinositides reach an upper steady state  $\pi_{III}(u(\xi))$ , at the site of the perturbation and a lower steady state  $\pi_{II}(u(\xi))$ , at all other regions of the membrane. The interface that should exist at the point of discontinuity corresponds to the inner solution to the problem.

### Inner Solution

In the previous section,  $\delta_p \frac{d^2 \pi}{d\xi^2}$  was assumed negligible. This assumption yielded a discontinuity in  $\pi$ , at  $\xi = \xi_{B,B'}$ . However, the true solution to the problem (for  $\delta_p \neq 0$ ) actually has a sharp interface in this region (see Figure 3-1b). This discrepancy occurs because  $\delta_p \frac{d^2 \pi}{d\xi^2}$  has been neglected in the region of sharp change. A regular perturbation analysis does not pick up the singular change near  $\xi = \xi_{B,B'}$ . In fact, it shrinks the region to a point.

In order to handle this difficulty another solution needs to be found near  $\xi = \xi_{B,B'}$ . This can be done by stretching the  $\xi$  coordinate in the region and imposing boundary

conditions that the solution should approach the outer solution as we move on either side of  $\xi = \xi_{B,B'}$ . On rescaling the region near  $\xi = \xi_{B,B'}$  as

$$y = \frac{\xi - \xi_{B,B'}}{\sqrt{\delta_p}} \quad (3.32)$$

equations (3.10) and (3.11) can be reduced to

$$\frac{d^2 \pi^i}{dy^2} = f(\pi^i, t^i) \quad (3.33)$$

$$\frac{d^2 t^i}{dy^2} = \delta_p g(\pi^i, t^i) \quad (3.34)$$

Here the superscript ‘ $i$ ’ denotes the inner solution to the problem. Using regular perturbation expansions in small parameter  $\delta_p$  for  $\pi^i \equiv \pi_0^i + \delta_p \pi_1^i \dots$  and  $t^i \equiv t_0^i + \delta_p t_1^i \dots$ , the zeroth order equations for (3.33) and (3.34) can be written as

$$\frac{d^2 \pi^i}{dy^2} = f(\pi^i, t^i) \quad (3.35)$$

$$\frac{d^2 t^i}{dy^2} = 0 \quad (3.36)$$

Note here, that the small term on this length scale is  $\delta_p g(\pi^i, t^i)$  and not the second derivative term. The denominator of (3.32),  $\sqrt{\delta_p}$ , is a small quantity. Therefore, a large change in  $y$  is required to shift  $\xi$  on either side of  $\xi_{B,B'}$ . Moving slightly to the left, say  $\xi = \xi_{B,B'} - \epsilon$ , translates to  $y \rightarrow -\infty$ . Similarly,  $\xi = \xi_{B,B'} + \epsilon$  translates to  $y \rightarrow \infty$ .

Now, consider the region around  $\xi = \xi_B$ . Continuity of the zeroth order inner and outer solution ensures that

$$\pi^i(-\infty) = \pi_i(t^i) \quad (3.37)$$

$$\pi^i(+\infty) = \pi_m(t^*) \quad (3.38)$$

$$t^i(-\infty) = t^i(+\infty) = t^* \quad (3.39)$$

Using (3.36) and boundary condition (3.39), we can get  $t^i(y) = t^*$ .

The unknown parameter  $t^*$  can be found using the continuity conditions (3.37) and (3.38). Multiplying (3.35) by  $\frac{d\pi^i}{dy}$ , integrating from  $-\infty$  to  $+\infty$  and using

$\frac{d\pi^i}{dy}(\pm\infty) \rightarrow 0$ , we get

$$\frac{1}{2} \left( \frac{d\pi^i}{dy} \right)^2 \Big|_{-\infty}^{+\infty} = 0 = \int_{\pi_m(t^*)}^{\pi^i(t^*)} f(\pi^i(y), t^*) d\pi^i \quad (3.40)$$

Equation (3.40) has the following physical interpretation. During the second stage of evolution, the sharp interface moves outward like a traveling wave due to an accumulation of phosphoinositides. As the wave propagates outward, the local concentration of the inositol phosphates ( $t^*$ ) keeps changing. When the phosphoinositides within the interface are produced at the same rate as they are removed (i.e., when (3.40) is satisfied), the wave stops propagating and forms a stationary front. This balance in phosphoinositide synthesis and removal, determines the width of the phosphoinositide localization.

In order to solve the inner solution to the problem, (3.35) can be rewritten in the form

$$\frac{d\pi^i}{dy} = \pm \sqrt{2(E - \phi_\pi)} \quad (3.41)$$

where  $\phi_\pi = - \int_{\pi}^{\pi^i} f(\pi^i, t^*) d\pi$  is the potential of the system and  $E(\pi^i, \pi_y^i)$  is the

Hamiltonian. Using (3.41), we can draw the phase plane of (3.35), for  $t = t^*$ . Any orbit on

this phase plane that satisfies (3.40) and the boundary conditions (3.37), (3.38) is a valid inner solution to the problem. Equation (3.40) implies that  $\phi_{\pi_I(t^*)} = \phi_{\pi_{III}(t^*)}$ . This in turn implies that  $E(\pi_I(t^*), 0) = E(\pi_{III}(t^*), 0)$ . The only orbit that can satisfy all these above conditions is a heteroclinic orbit,  $\pi^{I-}(y)$ , (AB, Figure 3-7) that connects the two saddle points,  $\pi_I(t^*)$  and  $\pi_{III}(t^*)$ . Similarly, the inner solution at  $\xi_{B'}$  corresponds to the heteroclinic orbit,  $\pi^{I+}(y)$ , (BA, Figure 3-7) that connects  $\pi_{III}(t^*)$  to  $\pi_I(t^*)$ .

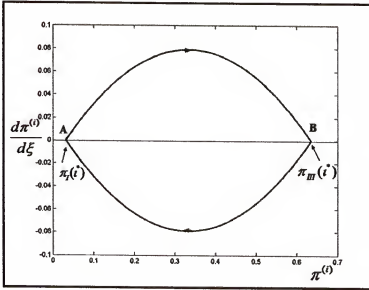


Figure 3-7. Heteroclinic orbit (AB) representing inner solution  $\pi^I(y)$ .

### Zeroth Order Approximation to Complete Solution

The zeroth order solution (see Figure 3-8) to the polarization subsystem (3.1), (3.2) can be found by patching up the inner and outer solutions. Using the fact that the inner solution asymptotically approaches constant values,  $\pi_I(\xi_{B,B'})$  or  $\pi_{III}(\xi_{B,B'})$  on either side of the sharp interface, the zeroth order solution,  $\pi_c(\xi)$ , can be written as

$$\pi_c(\xi) = \begin{cases} \pi_I(\xi) + \pi^{(I)-} \left( \frac{\xi - \xi_B}{\sqrt{\delta_p}} \right) - \pi_I(\xi_B) & 0 \leq \xi \leq \xi_B \\ \pi_{III}(\xi) + \pi^{(I)-} \left( \frac{\xi - \xi_B}{\sqrt{\delta_p}} \right) - \pi_{III}(\xi_B) & \xi_B \leq \xi \leq 1/2 \\ \pi_{III}(\xi) + \pi^{(I)+} \left( \frac{\xi - \xi_{B'}}{\sqrt{\delta_p}} \right) - \pi_{III}(\xi_{B'}) & 1/2 \leq \xi \leq \xi_{B'} \\ \pi_I(\xi) + \pi^{(I)+} \left( \frac{\xi - \xi_{B'}}{\sqrt{\delta_p}} \right) - \pi_I(\xi_{B'}) & \xi_{B'} \leq \xi \leq 1 \end{cases} \quad (3.42)$$

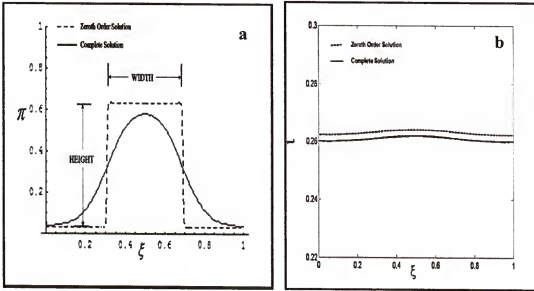


Figure 3-8. Zeroth order solutions (dashed lines) in comparison with the numerically calculated complete solution (solid lines). (a) Plot of  $\pi(\xi)$ . (b) Plot of  $t(\xi)$  (corresponds to orbit ABCB'A in Figure 3-5).

Since the inner solution  $t^{(I)}(\xi)$  is a constant,  $t^{(I)}(\xi_{B,B'}) = t^{(III)}(\xi_{B,B'}) = t^*$ , the zeroth order solution,  $t_c(\xi)$ , is nothing but the outer solution (Figure 3-8b)

$$t_c(\xi) = \begin{cases} t^{(I)}(\xi) & 0 \leq \xi \leq \xi_B \\ t^{(III)}(\xi) & \xi_B \leq \xi \leq \xi_{B'} \\ t^{(I)}(\xi) & \xi_{B'} \leq \xi \leq 1 \end{cases} \quad (3.43)$$



### Instability of the Homogenous Steady State with Respect to Change in $\kappa_f$

As discussed in Chapter 2, the homogenous resting state of the phosphoinositides evolves into a non-homogenous localization only when the synthesis rate of the phosphoinositides ( $\kappa_f$ ) is optimal. This property of gradient sensing can be analyzed by performing a Turing stability analysis to evaluate the stability of the homogenous steady state to non-homogenous perturbations, as  $\kappa_f$  is varied.

Consider the uniform resting state of the polarization subsystem  $(\tilde{\pi}, \tilde{t})$  i.e. the homogenous steady state obtained when no stimulus is applied to the model cell.  $\tilde{\pi}$  and  $\tilde{t}$  can be obtained from the following equations

$$f(\tilde{\pi}, \tilde{t}) = -(\kappa_f \tilde{\pi}^2 (1 - \tilde{\pi}) - \tilde{\pi} \tilde{t} + \psi_p - \kappa_p \tilde{\pi}) = 0 \quad (3.44)$$

$$g(\tilde{\pi}, \tilde{t}) = -(\kappa_f \tilde{\pi}^2 (1 - \tilde{\pi}) - \tilde{\pi} \tilde{t} + \psi_i - \kappa_i \tilde{\pi}) = 0 \quad (3.45)$$

In order to study the stability of the resting state, we may impose an arbitrarily small perturbation,  $\pi^*(\xi, \tau), t^*(\xi, \tau)$  to  $\tilde{\pi}$  and  $\tilde{t}$ , respectively. If the resting state is stable,  $\pi$  and  $t$  will return to their homogenous resting state  $(\tilde{\pi}, \tilde{t})$ . On the other hand, if the resting state is unstable,  $\pi$  and  $t$  will leave the resting state and evolve into another steady state in long-time. The equations that describe the evolution of these perturbations can be obtained by linearizing equations (3.5), (3.6) using  $\pi = \tilde{\pi} + \pi^*(\xi, \tau)$ ,  $t = \tilde{t} + t^*(\xi, \tau)$ , (3.44) and (3.45)

$$\frac{\partial \pi^*}{\partial \tau} = \delta_p \frac{\partial^2 \pi^*}{\partial \xi^2} - \pi^* (f'_\pi + f'_t) \quad (3.46)$$

$$\frac{\partial t^*}{\partial \tau} = \delta_i \frac{\partial^2 t^*}{\partial \xi^2} - t^* (g'_\pi + g'_t) \quad (3.47)$$

where  $f'_x, f'_i, g'_x, g'_i$  denote partial-derivatives evaluated at the resting state  $(\bar{\pi}, \bar{t})$ .

Now, the solution vector  $\bar{u} = (\pi^*, t^*)$  for (3.46),(3.47) can be expanded as a Fourier series expansion

$$\bar{u} = \begin{pmatrix} \pi^* \\ t^* \end{pmatrix} = \sum_j \bar{s}_j(\tau) \phi_j(\xi) \quad (3.48)$$

where  $\phi_j(x)$  denotes the  $j$ th eigenfunction of the eigenvalue problem<sup>4</sup>

$$-\frac{d^2 \phi_j(\xi)}{d\xi^2} = k_j^2 \phi_j(\xi) \quad (3.49)$$

with periodic boundary conditions  $\phi_j(0) = \phi_j(1)$  and  $\phi'_j(0) = \phi'_j(1)$ . Substituting the expansion (3.48) into (3.46) and (3.47), and equating the coefficients for each  $\phi_j(\xi)$ , we get the following problem for  $\bar{s}_j(\tau)$ ,

$$\frac{d\bar{s}_j}{d\tau} = M_j \bar{s}_j \text{ where } M_j \text{ denotes } \begin{pmatrix} -k_j^2 \delta_p - f_x & -f_i \\ -g_x & -k_j^2 \delta_i - g_i \end{pmatrix} \quad (3.50)$$

The solution to the linear problem (3.50) should be of the form  $c_1 \bar{v}_{j1} e^{\lambda_{j1}\tau} + c_2 \bar{v}_{j2} e^{\lambda_{j2}\tau}$ , where  $c_1, c_2$  are constants,  $\lambda_{j1}, \lambda_{j2}$  denote the eigenvalues of  $M_j$  and  $\bar{v}_{j1}, \bar{v}_{j2}$  denote the corresponding eigenvectors.

Since, each matrix  $M_j$  has two eigenvalues, the stability of the homogenous steady state depends on  $2 \times j$  eigenvalues,  $\lambda_{01}, \lambda_{02}, \lambda_{11}, \lambda_{12}$  etc. If any of these eigenvalues

---

<sup>4</sup> The eigenfunctions of the operator  $-d^2/d\xi^2$  have the form  $\phi_j(\xi) = \alpha_j e^{i k_j \xi}$ . Here,  $k_j$  represents non-negative eigenvalues or perturbation wavenumbers,  $2j\pi$  for  $j=0,1,2,\dots$

have positive real parts, the perturbation grows exponentially and the homogenous steady state becomes unstable. On the other hand if all the eigenvalues have negative real parts, the perturbation decays and the homogenous steady state is stable.

The eigenvalues for each  $M_j$  satisfies the characteristic equation

$$\lambda_j^2 + \lambda_j(f'_\pi + g'_i + k_j^2 \delta_p + k_j^2 \delta_i) + (k_j^4 \delta_p \delta_i + k_j^2 \delta_p g'_i + k_j^2 \delta_i f'_\pi + f'_\pi g'_i - f'_i g'_\pi) = 0$$

It follows that the stability of the homogenous steady state requires

$$\text{Trace}(M_j) = -(f'_\pi + g'_i + k_j^2 \delta_p + k_j^2 \delta_i) < 0 \quad (3.51)$$

$$\text{Det}(M_j) = (k_j^4 \delta_p \delta_i + k_j^2 \delta_p g'_i + k_j^2 \delta_i f'_\pi + f'_\pi g'_i - f'_i g'_\pi) > 0 \quad (3.52)$$

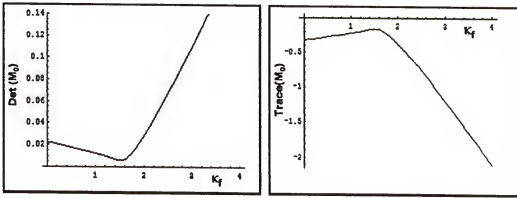


Figure 3-9. Plots of  $\text{Det}(M_0)$  and  $\text{Trace}(M_0)$  as parameter  $\kappa_f$  is varied.

First, consider the stability of the homogenous steady state with respect to spatially homogenous perturbations,  $\pi^+(\tau), i^+(\tau)$ . This corresponds to setting  $k=0$  and neglecting diffusion for  $\pi, i$ . In this case it turns out that as  $\kappa_f$  is varied, the conditions for stability,  $\text{Trace}(M_0) < 0$  and  $\text{Det}(M_0) > 0$ , are satisfied for all  $\kappa_f$  (see Figure 3-9). It also follows that there is only one unique steady state  $(\bar{\pi}, \bar{i})$  for each  $\kappa_f$ . This can be shown by using the following expressions

$$\frac{d\bar{\pi}}{d\kappa_f} = \frac{(f'_\pi g'_{\kappa_f} - g'_\pi f'_{\kappa_f})}{\text{Det}(M_0)} \quad (3.53)$$

$$\frac{d\bar{l}}{d\kappa_f} = \frac{(g'_\pi f'_{\kappa_f} - f'_\pi g'_{\kappa_f})}{\text{Det}(M_0)} \quad (3.54)$$

Since, the denominator of (3.53),(3.54) is always positive for all  $\kappa_f$ , the slope of the steady state curve can never reach infinity. Hence, as  $\kappa_f$  is varied, only one homogenous steady exists and this steady state is stable with respect to homogenous perturbations.

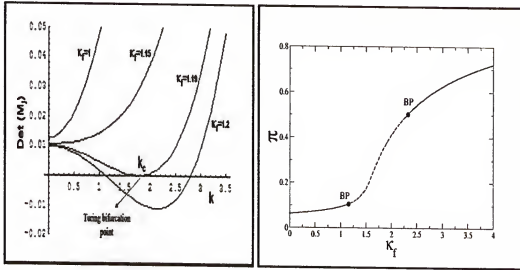


Figure 3-10. Turing bifurcation of the homogenous steady state. (a) Plot of  $\text{Det}(M_j)$  against  $k$ , for various values of  $\kappa_f$  values. Turing instability occurs when the  $k$  axis is tangential to the  $\text{Det}(M_j)$  curve. Here,  $k_c$  denotes the critical wave number at which instability occurs. (b) Bifurcation diagram for the homogenous steady state as  $\kappa_f$  is varied. Dashed line denotes the region of Turing instability; Solid line denotes stable steady states.

Using the above result, the Turing stability of the homogenous steady state to non-homogenous perturbations, can be analyzed using the conditions (3.51),(3.52) for all  $k$ . First, observe that condition (3.51) always holds as  $\kappa_f$  is varied. This follows from

$$\text{Trace}(M_j) = \text{Trace}(M_0) - (k_j^2 \delta_p + k_j^2 \delta_i) < 0 \quad (3.55)$$

because  $\text{Trace}(M_0) < 0$  and  $(k_j^2 \delta_p + k_j^2 \delta_i) > 0$ .

Hence, instability can occur only via condition (3.52). If we now assume that  $k$  is continuous, then the following conditions have to hold at the limit of stability (see Figure 3-10a)

$$\text{Det}(M_j) = 0 ; \frac{d\text{Det}(M_j)}{dk} = 0 \quad (3.56)$$

Condition (3.56) implies that the homogenous steady state is Turing unstable iff

$$\delta_p g'_i + \delta_i f'_e < -2 (\delta_p \delta_i \text{Det}(M_0))^{1/2} \quad (3.57)$$

This instability is realized with respect to perturbations whose wave number ( $k_{ej}$ , a discrete wave numbers among  $2j\pi$  for  $j=1,2,\dots$ ) is closest to  $k_e = (\delta_p \delta_i)^{-1/2} (\text{Det}(M_0))^{1/4}$ , the critical wave number at which condition (3.57) is valid (see Figure 3-10a).

Using (3.57), we can plot the bifurcation diagram for the homogenous steady state, as  $\kappa_f$  is varied (Figure 3-10b). As expected, the homogenous steady state becomes Turing unstable only at intermediate  $\kappa_f$ . Under these conditions, even the smallest non-homogenous fluctuation causes the homogenous steady state to lose stability and spontaneously polarize into a non-homogenous phosphoinositide distribution.

## CHAPTER 4 EXPERIMENTAL ANALYSIS

It has been shown in Chapter 2, that the model simulations are consistent with the spatiotemporal dynamics observed during gradient sensing. The specific aim of this chapter is to obtain experimental evidence that verifies the following fundamental hypotheses:

- Hypothesis 1: The spatiotemporal dynamics observed during gradient sensing are analogous to the dynamics of the activator-inhibitor class of reaction-diffusion models.
- Hypothesis 2: The membrane-resident phosphoinositides play the role of activator.

We can address both these hypotheses by experimentally studying the features of the continuation diagram (Figure 2-5). According to the model, when the mean chemoattractant concentration is small and the activator synthesis rate is slow, the inhibitor rapidly counteracts the synthesis of the activator and abrogates its polarization. When the chemoattractant concentration is high and the activator synthesis rate is fast; the inhibitor cannot contain the synthesis of the activator and causes the activator to propagate all over the membrane. Polarization of the activator can occur only at intermediate chemoattractant concentrations, when the synthesis rate of the activator is optimum. To test this feature, two classes of experiments have been performed using neutrophil-like HL60 cells [72],

- Biophysical Experiments: Cells have been exposed to a range of uniform chemoattractant concentrations and allowed to spontaneously polarize. The extent of polarity observed at each chemoattractant concentration has been quantified.

- **Biochemical Experiments:** These experiments determine whether changes in PI5K activity can regulate phosphoinositide synthesis and influence phosphoinositide polarization in a manner consistent with the model and with our choice of activator (membrane phosphoinositides).

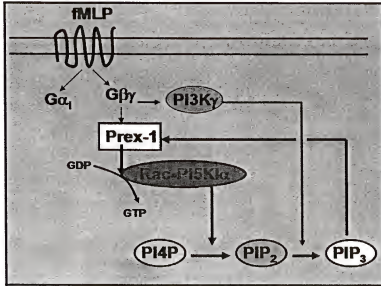


Figure 4-1. Kinetic scheme of the hypothesized positive feedback loop.

### The Positive Feedback Loop

Positive feedback is an essential component of the gradient sensing model.

Although there is evidence supporting positive feedback [48], the components of this feedback loop are yet to identified. Based on the current literature, one can construct the model shown in Figure 4-1.

In neutrophils, the receptors for the chemoattractant fMLP are coupled to membrane-resident G-proteins (see Figure 4-1). When a chemoattractant molecule binds to a receptor, the G-protein coupled to the receptor dissociates into its  $G\alpha_i$  and  $G\beta\gamma$  subunits. The  $G\beta\gamma$  binds and activates PI3K  $\gamma$  subunit, resulting in the synthesis of  $PIP_3$  from  $PIP_2$  [42, 73]. The  $PIP_3$  thus produced and the  $G\beta\gamma$  subunit, then synergistically activate the membrane-resident protein, P-Rex1, which belongs to the Dbl family of Rac-GEFs (guanine-nucleotide exchange factors for Rac) that activate Rac [45,

74]. In resting cells, Rac is cytosolic and GDP-bound. This state is maintained through its interaction with a GDP dissociation inhibitor (GDI) (Figure 4-2). Upon receptor activation, GDI dissociates from Rac by an unknown mechanism, and Rac-GDP targets to membrane via its C-terminal prenylation, where Rac-GEFs, such as P-Rex1, activate Rac by dissociating GDP and binding GTP [45]. To be sure, other Rac-GEFs of the Dbl family such as Tiam1 can also activate Rac, but P-Rex1 is most important insofar as its activity represents 65% of the total Rac-GEF activity in neutrophils [45].

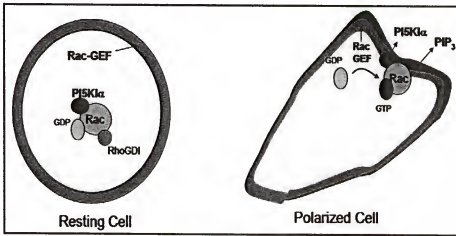


Figure 4-2. Components of the positive feedback loop in a resting cell and in a polarized cell.

*In vitro* experiments have shown that Rac interacts with the p85 subunit of PI3K  $\delta$  activity [46]. This has led to the suggestion that PIP<sub>3</sub> and Rac function in a positive feedback loop leading to rapid accumulation of PIP<sub>3</sub> [10, 48, 75]. However, *in vivo* data show that less than 1% of the total PI3K activity can be attributed to Rac-PI3K  $\delta$  [76].

A more plausible model for the closure of the positive feedback loop is the Rac-mediated activation of the enzyme PI5K, which catalyzes synthesis of PIP<sub>2</sub> from PI4P. Both GDP-bound and GTP-bound Rac interact with PI5K via their C-terminus [47, 58, 77, 78]. However, only GTP-bound Rac can activate PI5K [47, 78]. Based on these facts,



the following model is proposed (see Figure 4-1, Figure 4-2). Under resting conditions, a Rho-GDI/Rac-GDP/PI5K complex exists in the cytosol. Upon receptor activation, this Rho-GDI dissociates from the complex by an unknown mechanism and the Rac-GDP/PI5K complex gets recruited to the leading edge where Rac-GEFs convert Rac-GDP/PI5K to Rac-GTP/PI5K. Rac-GTP may either activate PI5K or provide PI5K access to its plasma membrane substrate, PI4P. This results in localized synthesis of PIP<sub>2</sub> at the plasma membrane. This increase in PIP<sub>2</sub> drives the formation of more PIP<sub>3</sub> and closes the feedback loop.

The forgoing model for the positive feedback loop is supported by several observations.

- Introduction of membrane permeant PIP<sub>3</sub> into resting neutrophils triggers the spontaneous polarization of endogenous PIP<sub>3</sub> [48]. However, if PI3K even membrane permeant PIP<sub>3</sub> cannot induce PIP<sub>3</sub> polarization. This implies that a functional positive loop is required for polarization, and PI3K is an essential component of this loop.
- Inhibition of PI3K results in loss of directionality, loss of PIP<sub>3</sub> localization and improper chemotaxis of neutrophils [30, 75, 79].
- Active Rac-GTP localizes at the leading edge of polarized neutrophils [80]. Overexpression of Rac-GTP results in PIP<sub>3</sub> accumulation all over the plasma membrane [49]. In contrast, Rac-GDP inhibits PIP<sub>3</sub> accumulation all over the plasma membrane. [49].
- In human fibroblasts, PI5KI $\alpha$  is cytosolic in serum-starved cells, but localizes to membrane ruffles upon growth factor stimulation [58]. However, inhibition of either PI5KI $\alpha$  or PI3K completely abolishes ruffle formation. Overexpression of Rac-GTP and PI5KI $\alpha$  results in an extensive ruffling phenotype, whereas disruption of the Rac-PI5KI $\alpha$  interaction results in inhibition of this phenotype. Similar effects of PI5K on actin polymerization have been observed in blood platelets [47]. These observations are consistent with our model where PI3K, PI5K and Rac are essential for positive feedback.
- *In vitro* experiments show that coexpression of PI5K and Rac-GTP markedly stimulates PI5K activity, whereas coexpression of PI5K and Rac-GDP inhibits PI5K activity [78, 81]. *In vivo* studies show that PI5K and Rac-GTP colocalize at

the plasma membrane and induce extensive actin polymerization. In contrast, PI5K and GDP-bound Rac fail to localize at the membrane and completely inhibit actin polymerization [81]. Thus, Rac regulates both the activity and the intracellular distribution of PI5K.

- Recent experiments have isolated a novel PI5K homolog called PIPKH [81]. This homolog does not possess PI5K activity, but acts as a scaffolding protein that binds to PI5Ks. Upon overexpression, PIPKH results in small increases in total  $PIP_2$  levels and dramatic increases in  $PIP_3$  levels. Consistent with the idea proposed in our model, the authors suggest that PIPKH recruits PI5K enzymes to specific intracellular sites where small increases in  $PIP_2$  levels induces massive accumulation of  $PIP_3$ .
- In HL60 cells, the C-terminus of Rac1 interacts with PI5K [77]. Introduction of the purified, membrane-permeant Rac1 C-terminus (without the effector region) inhibits the migration of HL60 cells. Consistent with our model, this inhibition occurs because the endogenous PI5K is saturated with inactive Rac1 C-terminus, and therefore cannot synthesize  $PIP_2$ . In contrast, when a C-terminal Rac1 mutant that does not bind to PI5K is introduced into HL60 cells, motility is normal. This observation highlights the importance of the Rac1-PI5K interaction in the positive feedback loop.

Taken together, these facts strongly suggest the positive feedback loop has the structure shown in Figure 4-1.

The biochemical experiments described in this chapter check if variation in PI5K activity regulates phosphoinositide polarity in a manner consistent with the model, the hypothesized positive feedback loop and the choice of our activator, membrane phosphoinositides.

HL60 cells, a human promyelocytic leukemia cell line, has been chosen as the model system to perform these experiments. When treated with dimethyl sulfoxide (DMSO) for 6–7 days, HL60 cells differentiate into neutrophil-like cells. They look and behave like neutrophils, orient their polarity in response to the chemoattractant, fMLP, and migrate in the right direction [18, 72]. The differentiated HL60 cells, referred to hereafter as *dHL60* cells, are easier to culture than the terminally differentiated

neutrophils. Moreover, HL60 cells have been the subject of numerous gradient sensing studies providing established benchmarks to test the validity of protocols used in this work.

### **Protocols**

The following protocols have optimized from earlier studies [18, 22, 30, 48, 82].

#### **Culturing and Differentiation of HL60 cells**

HL-60 cells ( $\sim 0.1 \times 10^6$  #/ml) are grown in RPMI 1640 medium (Sigma) containing HEPES buffer and supplemented with sodium bicarbonate, 10% FBS (Atlanta Biologicals) and Penicillin-Streptomycin-Glutamine (Invitrogen). The cells are allowed to grow in 8 ml of culture medium for 3-4 days until they reached a density of  $\sim 1.5 \times 10^6$  #/ml. Differentiation of the HL-60 cells to neutrophils is then induced by addition of 1.3% DMSO to  $\sim 3.0 \times 10^6$  cells in 20 ml culture medium. The cells are propagated for 7 days without changing the medium. Under these conditions, the suspended cells transform into neutrophil-like *d*HL60 cells.

#### **Transient Transfection by Electroporation**

An electroporation chamber (Model Series 1600, BRL-GIBCO) has been used for transient transfection. Six days after addition of DMSO,  $\sim 10^7$  *d*HL60 cells are washed once with serum-free RPMI-HEPES and resuspended in 200  $\mu$ l of the same medium. For single transfections, 30  $\mu$ g of plasmid DNA in 30  $\mu$ l of water is added to the cells. For double transfections, 50  $\mu$ g of the second plasmid is included. The cell-DNA mixture is incubated for 10 mins at room temperature, followed by 5 min incubation on ice. The mixture is transferred to the electroporation cuvettes, and then subjected to an electroporation pulse at 330V, 1000  $\mu$ F and 50  $\Omega$ . The transfected cells are allowed to

recover at room temperature for 10 minutes and subsequently transferred to 10 ml complete culture medium. Transfection efficiencies varied from about 5%-10% fluorescent cells, 16-24 hrs after electroporation.

## **Motility Assays**

### **Preparation of cells**

Differentiated HL-60 cells are washed once with 10 ml of serum free culture medium and resuspended in mHBSS solution (150mM NaCl, 4mM KCl, 1.2mM MgCl<sub>2</sub>, 10 mg/ml glucose, 20mM HEPES, 0.5% low endotoxin human serum albumin, pH 7.2, filter sterilized). The cells ( $\sim 0.3 \times 10^6$  total) are plated on the center of a sterile no. 1.5 coverslip rimmed with a square agarose spacer (Labtek). The coverslip was previously coated with 0.05mg/ml human fibronectin (BD Biosciences) and pre-blocked with 0.5% human serum albumin. After 30-40 minutes of incubation in a 37°C/5% CO<sub>2</sub> incubator, the non-adherent cells are removed by two washes with mHBSS/HSA. Cells are then incubated at RT for 5mins in 200µl of mHBSS/HSA.

### **Live cell imaging**

For point source stimulation, the cells are exposed to a 0.5µm micropipette (Eppendorf Femtotips) backfilled with 3µl of 10µM fMLP (Sigma) in mHBSS/HSA. The micropipette is placed in the microscope's field of view using a joystick-controlled micromanipulator (Zeiss). If necessary, a small backpressure is applied to the micropipette using a microinjector (Eppendorf) to release air bubbles. The pipette is then placed about 2-3 cell lengths away from a resting cell and allowed to passively diffuse chemoattractant. Subsequent events were captured at 10s intervals. For uniform

chemoattractant stimulation, 20 $\mu$ l of 10nM fMLP in mHBSS/HSA is gently added to coverslip instead.

Images are acquired using a cooled charged coupled device on a multiwavelength multi-wavelength wide-field three dimensional Delta Vision Restoration microscope (Olympus IX70) in which shutters, filter wheels, focus movement, and data collection are all computer driven. Cells are imaged using a  $60 \times 1.4$  N.A. lens (Olympus, Lake Success, NY) and  $n=1.514$  immersion oil. For fluorescence imaging of living cells, GFP, CFP or YFP signals are obtained on single optical sections (0.25 $\mu$ m) near the bottom of the cells. When necessary, differential interference contrast (DIC) images of the cells are simultaneously captured using a Nomarski system optimally aligned for our microscope system. Further image manipulation is done using Softworx, IVE or Adobe Photoshop Pro software.

### **Fixing and Immunostaining**

For uniform stimulation, 20 $\mu$ l of chemoattractant (10nM fMLP in mHBSS/HSA) is gently added to the coverslip. Cells are allowed to respond for a stipulated time and fixed for 20mins with 3.7% formaldehyde in freshly prepared cytoskeleton buffer containing 10mM HEPES, pH 7.2, 138mM KCl, 3mM MgCl<sub>2</sub>, 2mM EGTA and 0.32M sucrose. Cells are then washed once with cytoskeleton buffer and permeabilized for 2 minutes using 0.2% Triton-X 100 in cytoskeleton buffer without sucrose. For actin staining, cells are incubated for one hour in TxRed conjugated phalloidin (Molecular Probes) in PBS containing 1% goat serum, washed three times with PBS and mounted on glass slides.

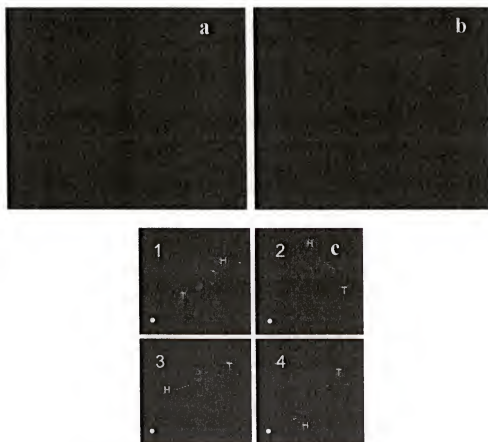


Figure 4-3. Spatiotemporal dynamics of PIP<sub>3</sub> localization in *dHL60* cells. (a) Image of a GFP-PH-Akt transfected *dHL60* cell moving towards a micropipette filled with 10 $\mu$ M sulphorhodamine (red) and 10 $\mu$ M fMLP. The GFP-PH-Akt localizes to the leading edge of the migrating cell. (b) A polarized, GFP-PH-Akt transfected *dHL60* cell migrating in response to a uniform bolus of 100nM fMLP. (c) A micropipette filled with 10 $\mu$ M fMLP (white circle) is placed towards the tail of a pre-polarized cell (frame 1). The cell responds by turning its leading edge in the direction of the micropipette (frames 2,3,4). 'H' denotes the head of the cell. 'T' denotes the tail.

For all other staining, permeabilized cells are incubated in a blocking solution (blotto) containing 50mM Tris-HCl, pH 7.5, 1mM CaCl<sub>2</sub> and 3% dry milk, followed by one hour incubation with an appropriate dilution of the primary antibody in blotto. After three successive washes in a solution containing 25mM Tris-HCl, pH 7.4, 140mM NaCl, 2.5mM KCl, and 1mM CaCl<sub>2</sub>, the cells are incubated for one hour with an appropriate dilution of the fluorescently labeled secondary antibody. After three successive washes

with the wash buffer, the stained cells are mounted on glass slides. Fluorescence images of the stained cells are acquired using the Delta Vision Restoration microscope.

## Results

### Biophysical Experiments

#### Spatiotemporal dynamics of gradient sensing

Previous biophysical studies on the dynamics of the PIP<sub>3</sub> localization in *dHL60* cells have shown the existence of spontaneous polarization and polarized sensitivity. The validity of the protocols used in the following experiments can be verified by first replicating these earlier studies. To this end, HL60 cells stably transfected with a marker of PIP<sub>3</sub>, GFP-PH-Akt (cell line from UCSF, Cell culture facility) were differentiated with 1.3% DMSO. Seven days after DMSO treatment, the differentiated cells were plated on coverslips, exposed to different types of chemoattractant profiles and the resulting response was observed.

- **Response to a chemoattractant gradient.** Cells plated on the coverslip were exposed to micropipette filled with 10 $\mu$ M of fMLP in mHBSS/HSA. The resting cell polarized in morphology and accumulated GFP-PH-Akt at its leading edge. This was followed by the persistent migration of the cell towards the pipette tip (Figure 4-3a).
- **Response to uniform chemoattractant concentrations.** Cells plated on the coverslip were exposed to a 100nM uniform concentration of fMLP in mHBSS/HSA. The GFP-PH-Akt construct accumulated at the plasma membrane within 1 min. Roughly 2 mins later, the GFP-PH-Akt polarized spontaneously at a random location on the cell membrane (Figure 4-3b).
- **Response to a switch in the direction of the chemoattractant gradient.** A micropipette filled with 10 $\mu$ M fMLP was placed at the tail of a pre-polarized cell. The cell exhibited polarized sensitivity – its leading edge turned towards the pipette tip (Figure 4-3c).

### Spontaneous polarization as a function of the chemoattractant concentration

To test the validity of the continuation diagram (Figure 2-5), *dHL60* cells were starved for 1 hour in mHBSS/HSA, plated on coverslips and exposed various uniform fMLP concentrations varying from 0.1nM to 100 $\mu$ M. After 2 minutes of treatment, the cells were fixed with 3.7% formalin, permeabilized and stained with rhodamine phalloidin, a marker for polymerized actin.

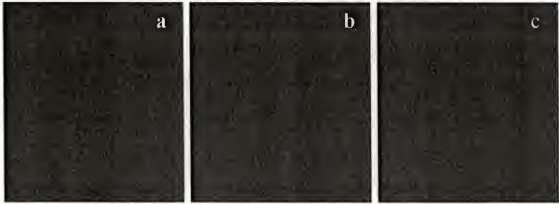


Figure 4-4. Spontaneous polarization as a function of chemoattractant concentration. Cells fixed two minutes after uniform fMLP treatment and stained with rhodamine phalloidin to visualize actin polymers. Scale bar, 20 $\mu$ m. (a) Low chemoattractant (0.1 nM fMLP). Very few cells showed actin polymerization at the membrane. (b) Intermediate chemoattractant (100 nM fMLP). Actin polymerization is confined at the leading edge of the cell. (c) High chemoattractant (100 $\mu$ M fMLP). Actin polymerization spreads all over the periphery of the cell.

Consistent with model predictions, at low concentrations of chemoattractant (0.1nM fMLP), cells did not show actin polymerization at the membrane (Figure.4-4a). However, at intermediate concentrations of chemoattractant (100nM fMLP), the cells polymerize actin exclusively at their leading edges (Figure 4-4b). At higher chemoattractant concentrations (100 $\mu$ M fMLP), cells lost their tails and showed actin polymerization all over the periphery of the cell (Figure 4-4c).



The polarity observed in each of these experiments, has been quantified by measuring the ratio of the cell perimeter showing intense phalloidin staining to the total cell perimeter. Results of this quantification have been shown in Figure 4-5.

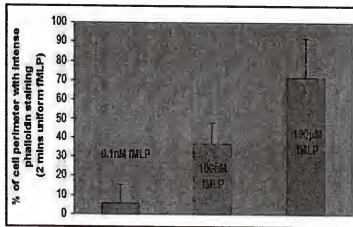


Figure 4-5. Quantification of polarity. ImageJ software was used to measure the ratio between the cell perimeter showing intense phalloidin staining and the total cell perimeter. Results are from two independent experiments and a total of 30 cells were counted in each experiment.

## Biochemical Experiments

### Role of PI5K in the Positive Feedback Loop

It has been proposed that PI5K is an element that completes the positive feedback loop for PIP<sub>3</sub> and PIP<sub>2</sub> synthesis. If this hypothesis is true, inhibition of PI5K activity should block the localization of PIP<sub>3</sub>. Overexpression of PI5K activity should cause propagation of PIP<sub>3</sub> all over the membrane.

Type I PI5K has three human isoforms PI5KI $\alpha$ , PI5K $\beta$  and PI5K $\gamma$ . Based on the study performed by [58], the PI5KI $\alpha$  isoform has been chosen for the experiments on HL60 cells. This study showed that in PDGF-stimulated human fibroblasts, only the PI5KI $\alpha$  isoform gets recruited to the membrane and plays a role in membrane ruffling. Both the other isoforms do not play a role in actin polymerization. The PI5K $\beta$  isoform

localized in the cytosolic region [58] and the PI5K $\gamma$  isoform associated with focal adhesions [83].

### **Construction of fluorescent PI5KI $\alpha$ mutants and Coronin**

In order to overexpress or inhibit PI5KI $\alpha$ , fluorescent cyan and yellow fusion proteins of full-length, human, PI5KI $\alpha$  and its inactive mutant, PI5KI $\alpha kn$  have been constructed. The PI5KI $\alpha kn$  mutant has two mutations in its catalytic domain, an Arg-427 to Gln (R427Q) and an Asp-309 to Asn(D309N). This inactive mutant, PI5KI $\alpha kn$ , has been shown to have <1% wild type PI5K activity [84]. PI5KI $\alpha kn$  inhibits PIP<sub>2</sub> synthesis by competing with the endogenous PI5KI $\alpha$ , for the substrate, PI4P.

The full length PI5KI $\alpha$  and its inactive mutant were subcloned by PCR from the pcDNA3-pFLAG vectors (gift from Dr. Richard Anderson, University of Wisconsin) into pCI-Neo-eYFP and pCI-Neo-eCFP mammalian expression vectors using BamHI and EcoRI cloning sites. All the PI5KI $\alpha$  inserts were confirmed by sequencing. The expression of YFP-PI5KI $\alpha$  in Cos7 cells was also confirmed by immunoblotting cell lysates with an anti-GFP antibody (Chemicon). In order to observe *de novo* actin polymerization in living cells, yellow fusion proteins of human Coronin 1 have also been constructed. Coronin is a 55 Kda protein that was isolated from the slime mould, *Dictyostelium* [85]. Coronin proteins are recruited from the cytosol to a nascent leading edge, where they participate in actin reorganization. Appropriate PCR has been used to insert the cDNA for the most abundant human Coronin homologue, Coronin 1 into the pCI-Neo-eYFP expression system. The expression of YFP-Coronin 1 in Cos7 cells has also confirmed by immunoblotting with the anti-GFP antibody.

### Assaying the efficacy of the fluorescent constructs in Cos7 cells

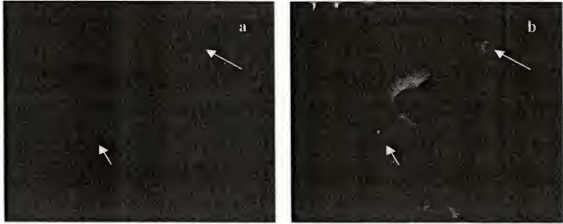


Figure 4-6. Distribution of endogenous PI5KI $\alpha$  in PDGF stimulated Cos7 cells. (a) Endogenous PI5KI $\alpha$  colocalizes with (b) YFP-Coronin1, at membrane ruffles (white arrows).

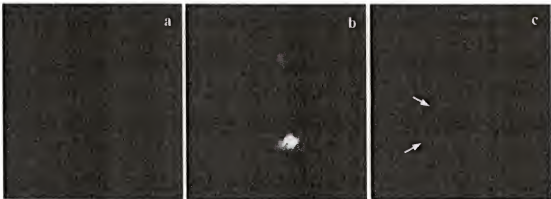


Figure 4-7. Ruffle inhibition in PI5KI $\alpha$ kn transfected Cos7 cells. Cells expressing both constructs, (a) CFP-PI5KI $\alpha$ kn and (b) YFP-Coronin1, showed no membrane ruffling or Coronin1 localization. In contrast cells transfected with only (c) YFP-Coronin1 showed normal membrane ruffling and Coronin1 localization (white arrows).

**Distribution of endogenous PI5KI $\alpha$  in Cos7 cells.** Cos7 fibroblasts were transfected with the YFP-Coronin1 (marker for polymerized actin) construct using a Superfect transfection kit (Qiagen). These cells were then serum starved for 24 hours, stimulated with 20 ng/ml PDGF, fixed and stained with a polyclonal PI5KI $\alpha$  antibody (gift from Dr. Richard Anderson, University of Wisconsin). Images of these cells show

that endogenous PI5KI $\alpha$  (Figure 4-6a) colocalized with YFP-Coronin1 (Figure 4-6b) at membrane ruffles.

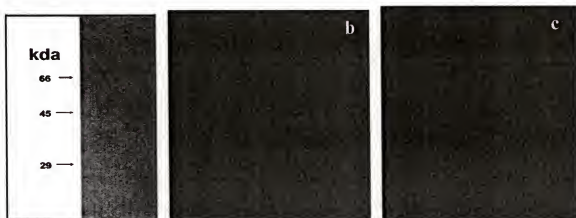


Figure 4-8. Expression and distribution of PI5KI $\alpha$  in dHL60 cells. (a) dHL60 lysates were probed for ubiquitous expression of PI5KI $\alpha$  using 1 $\mu$ g polyclonal anti-PI5KI $\alpha$ . A 68 kda protein corresponding to PI5KI $\alpha$  was found. (b and c) GFP-PH-Akt transfected cell dHL60 cells were stimulated with 100nM fMLP. Cells were fixed and stained with 3 $\mu$ g of anti-PI5KI $\alpha$  antibody. Both GFP-PH-Akt (b) and PI5KI $\alpha$  (c) enriched ruffles at the leading edge of the cell.

**PI5KI $\alpha$ kn inhibits ruffles.** [58] showed that the PI5KI $\alpha$ kn, inhibits actin polymerization in human fibroblasts treated with PDGF. This experiment has been reproduced to check the efficacy of the PI5KI $\alpha$ kn construct. Cos7 cells were cotransfected with YFP-Coronin1 and the inactive mutant, CFP-PI5KI $\alpha$ kn, at a 1:3 ratio. In serum-starved cells, CFP-PI5KI $\alpha$ kn localized predominantly at the Golgi (which is consistent with the results in [81]). Upon stimulation with 20ng/ml PDGF, CFP-PI5KI $\alpha$  was recruited all over the periphery of the cell (Figure 4-7a). However, 87% of the cells transfected with both CFP-PI5KI $\alpha$ kn and YFP-Coronin1, did not show any membrane ruffling or Coronin1 localization (Figure 4-7a,b). In contrast, 71% of the cells transfected with only YFP-Coronin1, showed normal ruffling and Coronin1 localization (Figure 4-7c). These results indicate that the PI5KI $\alpha$ kn construct is functioning properly.

### Expression and distribution of PI5KI $\alpha$ in *dHL60* cells

Before studying the role of PI5KI $\alpha$  in *dHL60* cells, it was imperative check if the  $\alpha$  isoform of Type I PI5K was expressed in *dHL60* cells. Hence, *dHL60* cell lysates were probed for PI5KI $\alpha$  using the polyclonal PI5KI $\alpha$  antibody. The western blot isolated a band corresponding to the 68 kda PI5KI $\alpha$  (Figure 4-8a). This confirmed the expression of PI5KI $\alpha$  in *dHL60* cells.

The distribution of endogenous PI5KI $\alpha$  in *dHL60* cells was also studied. GFP-PH-Akt transfected stables were treated with 100nM chemoattractant fMLP, fixed and stained with the polyclonal PI5KI $\alpha$  antibody. Both GFP-PH-Akt (Figure 4-8b) and PI5KI $\alpha$  (Figure 4-8c) were predominantly found in membrane ruffles at the leading edge of the cell.

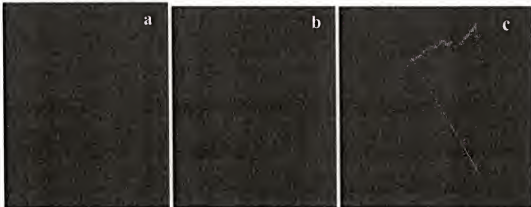


Figure 4-9. Overexpression of PI5K. Cell transfected with GFP-PH-Akt and CFP-PI5KI $\alpha$  was exposed to 100nM uniform fMLP. (a) GFP-PH-Akt and (b) CFP-PI5KI $\alpha$  colocalized all over cell membrane. (c) Cell transfected with only GFP-PH-Akt, localizes the probe at its leading edge. Scale bar, 20 $\mu$ m. Graphs in the background indicate the fluorescence intensity along the line drawn across the cell.

### PI5K1 $\alpha$ regulates PIP<sub>3</sub> polarity in dHL60 cells

The aim of this experiment was to check if regulation of PI5K activity could influence PIP<sub>3</sub> polarization. GFP-PH-Akt and CFP-PI5K1 $\alpha$  (either the full length or the inactive construct) were cotransfected into dHL60 cells by electroporation<sup>4</sup>, six days after DMSO treatment. After about 24 hours, 5-10% of the cells expressed at least one of the constructs. However, nearly 75% of the transfected cells expressed both the constructs. Cells were then plated on coverslips and stimulated with 100nM uniform fMLP.

**Overexpression of PI5K.** When cells transfected with both CFP-PI5K1 $\alpha$  and GFP-PH-Akt were exposed to uniform fMLP, both the constructs failed to polarize. Instead, both the constructs colocalized all over the periphery of the cell (Figure 4-9a,b). These cells were neither able to morphologically polarize, nor migrate. In contrast, cells that were transfected with only GFP-PH-Akt, polarized normally and showed GFP-PH-Akt localization at the leading edge (Figure 4-9c).



Figure 4-10. Control experiment. Cell transfected with GFP (without PH-Akt) and CFP-PI5K1 $\alpha$  was exposed to 100nM uniform fMLP. (a) GFP (no insert) did not

<sup>4</sup>Direct microinjection of the constructs into the cell would have provided a more reliable way of transfecting the cells. In this case, expression of the constructs would take a short time and would have limited side effects on the normal function of the cell. However, the small size of the dHL60 cells (~10 $\mu$ m) make microinjection difficult. Hence, electroporation has been used.

localize at the cell membrane. However, (b) CFP-PI5K1 $\alpha$  colocalized all over cell membrane. Scale bar, 11 $\mu$ m.

The colocalization observed in Figure 4-9a,b was not an artifact resulting from plasma membrane folding. This was confirmed by cotransfecting *dHL60* cells with CFP-PI5K-WT and GFP (without PH-Akt). Although CFP-PI5K $\alpha$  (Figure 4-10b) accumulated all over the periphery of the cell, GFP (Figure 4-10a) remained in the cytosolic region.



Figure 4-11. Inhibition of PI5K. Cell transfected with GFP-PH-Akt and inactive, CFP-PI5K1 $\alpha$ kn was exposed to 100nM uniform fMLP. (a) GFP-PH-Akt did not localize at any part of the membrane (b) CFP-PI5K1 $\alpha$  localized all over cell membrane and at the golgi. Scale bar, 20 $\mu$ m. Graphs in the background indicate the fluorescence intensity along the line drawn across the cell.

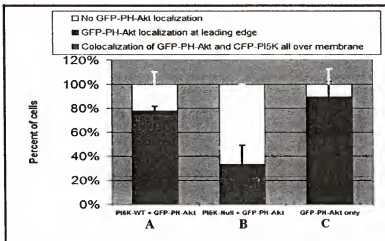


Figure 4-12. PI5K regulation of PIP<sub>3</sub> polarization –Quantification of study.

**Inhibition of PI5K.** Cells cotransfected with the inactive, CFP-PI5KI $\alpha$ kn and GFP-PH-Akt, were exposed to fMLP and images in the CFP and GFP channels were obtained. CFP-PI5KI $\alpha$ kn localized all over the periphery of the cell and at in the golgi (Figure 4-11b). However, GFP-PH-Akt failed to localize at any portion of the cell membrane (Figure 4-11a). This shows that PI5KI $\alpha$  is critical for the polarization of GFP-PH-Akt. Interestingly, these cells were still able to polarize and migrate. Cells transfected with only GFP-PH-Akt, showed normal polarization of the probe upon treatment with fMLP.

Quantification of the PI5K studies indicate that nearly 90% of the cells transfected only with GFP-PH-Akt showed normal PIP<sub>3</sub> polarization (Figure 4-12c). However, when PI5KI $\alpha$  was overexpressed, nearly 80% of the cotransfected cells localized GFP-PH-Akt all over the cell membrane (Figure 4-12a). In contrast, when PI5KI $\alpha$  was inhibited, 65% of the cotransfected cells did not show GFP-PH-Akt localization at the membrane (Figure 4-12b).

These results support the hypothesis that PI5KI $\alpha$  is involved in a positive feedback loop for generation of PIP<sub>3</sub>. They also indicate that PI5KI $\alpha$  regulates PIP<sub>3</sub> polarization in a manner consistent with the model characteristics shown in Figure 2-5.

It is important to note that these experiments do not categorically prove the role of PI5KI $\alpha$  in a positive feedback loop for PIP<sub>3</sub> synthesis. This hypothesis can be verified by inhibiting PI5KI $\alpha$ , and then introducing membrane permeant PIP<sub>3</sub> into cells to check if PIP<sub>3</sub> can still trigger its own synthesis.



## CHAPTER 5 CONCLUSIONS

A simple reaction-diffusion model based on the phosphoinositide cycle can effectively capture the spatiotemporal dynamics involved in gradient sensing. The model consists of two subsystems: (1) Adaptation subsystem that is activated on a fast time scale and inhibited on a slow time scale. (2) Polarization subsystem that consists of a slow diffusing, autocatalytic activator and a fast diffusing inhibitor. Although there is some evidence supporting the choice of activator (membrane phosphoinositides) and inhibitor (inositol phosphates), more experiments need to be performed to categorically prove the identity of these species. However, the success of this model suggests that the molecular players, whatever be their identity should possess the properties of the variables in the model. The features exhibited by the model are summarized below.

### Fast Responses

1. **Phosphoinositide localization.** Exposure of a cell to a shallow chemoattractant gradient results in the translocation of phosphoinositides to the leading edge of the cell. Receptor-ligand binding activates the model and nullifies the threshold required for the amplification of membrane phosphoinositides. This results in the synthesis of phosphoinositides at the leading edge. The rapid diffusion of the inositol phosphates from the leading edge to the trailing edge inhibits the build up of phosphoinositides at the back of the cell and restricts the phosphoinositide localization to the front of the cell.
2. **Unique localization.** When the cell is exposed to two unequal sources of chemoattractant, phosphoinositides localize towards both sources initially. However, as time progresses, only the localization at the stronger site persists. Thus, the model demonstrates that the cell can migrate only along a unique direction regardless of the chemoattractant stimulus.
3. **Properties of the localization.** The geometry of the phosphoinositide distribution varies with the shape of the chemoattractant profile. The phosphoinositide

distribution also depends on the mean value of the chemoattractant concentration. Small or large mean values yield a nearly uniform phosphoinositide distribution. Intermediate mean values result in a pronounced phosphoinositide localization. The width of the phosphoinositide peak increases with the mean value.

4. **Polarized sensitivity.** When a polarized cell is exposed to a modest chemoattractant gradient along a new direction, a new localization does not develop at the point of highest chemoattractant concentration. Instead, the existing localization turns towards the new stimulus. If the new gradient is localized and steep enough to overcome the existing threshold, a new localization is generated and the existing localization is disrupted. If the polarized cell is exposed to a new gradient that is superimposed on a pre-existing gradient, the response observed depends on the original gradient, the intensity of the pre-existing polarity and the shape of the new gradient.

### Slow Responses

1. **Adaptation.** When a cell that is being exposed to a uniform chemoattractant concentration is subjected to a higher uniform chemoattractant concentration, there is a rapid increase in phosphoinositides along the entire cell membrane. This increase is followed by a slow decline in the phosphoinositides back to its initial distribution. We have captured this response by assuming that a hypothetical component gets activated on a fast time scale and inhibited on a slow time scale. The model assumes that this hypothetical component drives phosphoinositide synthesis.
2. **Spontaneous polarization.** Experiments show that cells exposed to a uniform concentration of chemoattractant polarize before adaptation is complete. To account for this property, we assume that the chemoattractant concentration undergoes stochastic fluctuations. If the mean concentration of the chemoattractant is large enough to overcome the threshold, the uniform phosphoinositide distribution develops into a phosphoinositide peak at a random location on the cell membrane. As time progresses, the cell adapts, the rate of phosphoinositide synthesis decreases, and the peak disrupts.

All the above responses clearly preclude the hypothesis that the cell merely amplifies the external signal. Instead, this model indicates that the cell must be viewed as a system that non-linearly processes chemoattractant inputs. It has been shown in particular that these complex dynamics can be explained very simply in terms of the instabilities and wavefront dynamics that are characteristic of the activator-inhibitor model.

The evolution of the phosphoinositide localization consists of two distinct phases. During the first phase, the region of the membrane that crosses the threshold gets amplified to a higher steady state. All other regions the cell get inhibited to a lower steady state. The formation of these two “plateaus” result in a large transition layer where there is accumulation of phosphoinositides. This accumulation of phosphoinositides drives the outward motion of the transition layer until there is a zero net-flux of phosphoinositides within the layer.

A zeroth order approximation to the steady state solution has been derived by utilizing the difference in diffusion between the activator and inhibitor. Perturbation techniques were used to arrive at separate inner and outer solutions to the problem. The two solutions were then patched up to obtain the steady state response. Geometrical properties of the response, such as height and width have also been derived.

A Turing stability analysis of the homogenous resting state has been performed. This analysis gives insight into the conditions required for the homogenous steady to lose stability and spontaneously polarize into a phosphoinositide localization. It has been found that this phenomenon occurs only when the synthesis rate of the phosphoinositides is at an optimum.

Finally, experiments have been performed to justify the choice of this class of activator-inhibitor models to explain gradient sensing. This has been done by testing the following model result: phosphoinositide polarization is possible only when the phosphoinositide synthesis rate is optimum. This result has been tested by performing (a) biophysical experiments where *dHL60* cells were exposed to a range of uniform fMLP concentrations, and fixed after 2 minutes. Actin polarized only at an intermediate

concentration of chemoattractant (100nM). At high concentrations (100 $\mu$ M), actin polymers were observed all over the cell membrane and at low concentrations (0.1nM) the response was completely lost. (b) biophysical experiments where the activity of PI5KI $\alpha$  in *aHL60* cells was altered to study the direct influence of phosphoinositide synthesis on phosphoinositide polarization. As expected, overexpression of PI5KI $\alpha$  resulted in the propagation of phosphoinositides all over the plasma membrane and inhibition resulted in abrogation of the phosphoinositide response. This study also supports the involvement of PI5KI $\alpha$  in a positive feedback loop.

# APPENDIX A NOMENCLATURE

Table A-1. Model parameters.

Parameter	Definition
$c_i$	Basal synthesis rate of inositol phosphates
$c_p$	Basal synthesis rate of phosphoinositides
$C$	Circumference of the cell
$D_i$	Lateral diffusivity of inositol phosphates
$D_p$	Lateral diffusivity of phosphoinositides in plasma membrane
$D_{p_e}$	Lateral diffusivity of phosphoinositides in endoplasmic reticulum
$k_f$	Rate constant for receptor mediated phosphoinositide formation
$k_r$	Rate constant for removal of phosphoinositides
$k_p$	Rate constant for basal degradation of phosphoinositides
$k_i$	Rate constant for basal degradation of inositol phosphates
$k^+$	Rate constant for receptor-ligand association
$k^-$	Rate constant for receptor-ligand dissociation
$r$	Concentration of active ligand bound receptor
$p$	Concentration of membrane phosphoinositides
$i$	Concentration of inositol phosphates
$p_e$	Concentration of phosphoinositides in endoplasmic reticulum
$l$	Concentration of ligand
$r_{p,f}$	Rate of formation of membrane phosphoinositides
$r_{p,r}$	Rate of removal of membrane phosphoinositides
$r_{p,d}$	Degradation rate of membrane phosphoinositides
$r_{i,d}$	Degradation rate of inositol phosphates
$R$	Radius of the cell
$s$	Membrane length per unit cell area
$a$	Time scale for evolution of component $U$
$b$	Time scale for evolution of component $V$
$r_t$	Concentration of total receptors

Table A-2. Greek symbols

Symbol	Definition
$\psi_i$	Dimensionless rate of basal synthesis of inositol phosphates
$\psi_p$	Dimensionless rate of basal synthesis of phosphoinositides
$\delta_i$	Dimensionless angular diffusivity of inositol phosphates
$\delta_p$	Dimensionless angular diffusivity of phosphoinositides in plasma membrane
$\delta_{p_r}$	Dimensionless angular diffusivity of phosphoinositides in endoplasmic reticulum
$\kappa_f$	Dimensionless rate constant for receptor mediated phosphoinositide formation
$\kappa_p$	Dimensionless rate constant for basal degradation of phosphoinositides
$\kappa_i$	Dimensionless rate constant for basal degradation of inositol phosphates
$\kappa^-$	Dimensionless rate constant for receptor-ligand dissociation
$\rho$	Dimensionless concentration of active receptor
$\pi$	Dimensionless concentration of phosphoinositides in plasma membrane
$l$	Dimensionless concentration of inositol phosphates
$\pi_s$	Dimensionless concentration of phosphoinositides in endoplasmic reticulum
$\lambda$	Dimensionless concentration of ligand
$\tau$	Dimensionless time
$\tau_r$	Dimensionless time constant for receptor-ligand binding
$\tau_u$	Dimensionless time constant for evolution of $U$
$\tau_v$	Dimensionless time constant for evolution of $V$
$\xi$	Angular coordinate scaled between 0 and 1

## APPENDIX B ORDERS OF MAGNITUDE OF PARAMETERS

The orders of magnitude of the parameters in Table 2-1 were based on the following experimental observations:

1. Under receptor-activated conditions, the turnover time of membrane phosphoinositides is 2 seconds [51]; hence:

$$k_f p_i^2, k_r s p_i \sim 1 \text{ sec}^{-1} \Rightarrow \kappa_f \mu \equiv \frac{k_f p_i^2}{k_r s p_i} \sim 1.0$$

5. Under unstimulated conditions, the turnover time of membrane phosphoinositides is 300 seconds [51]; hence,

$$c_p/p_i \sim 0.01 \text{ sec}^{-1} \Rightarrow \psi_p \equiv \frac{c_p/p_i}{k_r s p_i} \sim 0.01$$

6. Under unstimulated conditions, the membrane contains 10–30% of the phosphoinositides in the endoplasmic reticulum ( $\pi \sim 0.1$ ). Since the phosphoinositide cycle turns slowly under these conditions, the phosphoinositide concentration is determined by degradation and *de novo* synthesis. It follows that,

$$\kappa_p \pi = \psi_p \Rightarrow \kappa_p \sim 0.1$$

7. No parameter values could be found for  $\psi_i$ . It was assumed that:

$$\psi_i = \psi_p = 0.01$$

This is tantamount to assuming that under basal conditions, the turnover time of the inositol phosphate pool is on the order of 100 seconds.

8. Under basal conditions, the inositol phosphate pool constitutes 40% of the phosphoinositides in the cell ( $i \sim 0.1$ ) [86]; hence:

$$\kappa_i i = \psi_i \Rightarrow \kappa_i \sim 0.1$$

9. The lateral diffusivity of cytosolic  $\text{I}(1,4,5)\text{P}_3$  is  $2.8 \times 10^{-6} \text{ cm}^2 \text{ sec}^{-1}$  [86]. Since the cell diameter is on the order of  $10^{-3} \text{ cm}$  [87],

$$D_l/C^2 \sim 1 \text{ sec}^{-1} \Rightarrow \delta_l \equiv \frac{D_l/C^2}{k_r s p_l} \sim 1.0$$

10. The lateral diffusivity of membrane phospholipids is on the order of  $10^{-9} \text{ cm}^2 \text{ sec}^{-1}$  [15]; thus:

$$D_p/C^2 \sim 10^{-3} \text{ sec}^{-1} \Rightarrow \delta_p \equiv \frac{D_p/C^2}{k_r s p_l} \sim 10^{-3}$$

11. The diffusivity of the stored phosphoinositides has been assumed to be the same as that of the membrane phosphoinositides:

$$\delta_{p_s} \equiv \frac{D_{p_s}/C^2}{k_r s p_l} \sim 10^{-3}$$



## LIST OF REFERENCES

- [1] D Bray, *Cell movements*. New York: Garland, 1992.
- [2] GE Jones, "Cellular signaling in macrophage migration and chemotaxis," *J Leukoc Biol*, vol. 68, pp. 593-602, 2000.
- [3] P Martin, "Wound healing--aiming for perfect skin regeneration," *Science*, vol. 276, pp. 75-81, 1997.
- [4] MA Moore, "The role of chemoattraction in cancer metastases," *Bioessays*, vol. 23, pp. 674-6, 2001.
- [5] DA Lauffenburger and AF Horwitz, "Cell migration: a physically integrated molecular process," *Cell*, vol. 84, pp. 359-69, 1996.
- [6] OD Weiner, "Regulation of cell polarity during eukaryotic chemotaxis: the chemotactic compass," *Curr Opin Cell Biol*, vol. 14, pp. 196-202, 2002.
- [7] RT Tranquillo, DA Lauffenburger, and SH Zigmond, "A stochastic model for leukocyte random motility and chemotaxis based on receptor binding fluctuations," *J Cell Biol*, vol. 106, pp. 303-9, 1988.
- [8] TD Coates, RG Watts, R Hartman, and TH Howard, "Relationship of F-actin distribution to development of polar shape in human polymorphonuclear neutrophils," *J Cell Biol*, vol. 117, pp. 765-74, 1992.
- [9] AL Hall, A Schlein, and J Condeelis, "Relationship of pseudopod extension to chemotactic hormone-induced actin polymerization in amoeboid cells," *J Cell Biochem*, vol. 37, pp. 285-99, 1988.
- [10] P Rickert, OD Weiner, F Wang, HR Bourne, and G Servant, "Leukocytes navigate by compass: roles of PI3Kgamma and its lipid products," *Trends Cell Biol*, vol. 10, pp. 466-73, 2000.
- [11] CA Parent and PN Devreotes, "A cell's sense of direction," *Science*, vol. 284, pp. 765-70, 1999.
- [12] HJ Song and MM Poo, "Signal transduction underlying growth cone guidance by diffusible factors," *Curr Opin Neurobiol*, vol. 9, pp. 355-63, 1999.
- [13] M Sohrmann and M Peter, "Polarizing without a c(l)ue," *Trends Cell Biol*, vol. 13, pp. 526-33, 2003.
- [14] R Wedlich-Soldner and R Li, "Spontaneous cell polarization: undermining determinism," *Nat Cell Biol*, vol. 5, pp. 267-270, 2003.
- [15] JM Haugh, F Codazzi, M Teruel, and T Meyer, "Spatial sensing in fibroblasts mediated by 3' phosphoinositides," *J Cell Biol*, vol. 151, pp. 1269-1279, 2000.
- [16] CA Parent, BJ Blacklock, WM Froehlich, DB Murphy, and PN Devreotes, "G protein signaling events are activated at the leading edge of chemotactic cells," *Cell*, vol. 95, pp. 81-91, 1998.

- [17] R Meili, C Ellsworth, S Lee, TBK Reddy, H Ma, and RA Firtel, "Chemoattractant-mediated transient activation and membrane localization of Akt/PKB is required for efficient chemotaxis to cAMP in Dictyostelium," *EMBO J.*, vol. 18, pp. 2092-2105, 1999.
- [18] G Servant, OD Weiner, P Herzmark, T Balla, JW Sedat, and HR Bourne, "Polarization of chemoattractant receptor signaling during neutrophil chemotaxis," *Science*, vol. 287, pp. 1037-40, 2000.
- [19] L Cassimeris and SH Zigmond, "Chemoattractant stimulation of polymorphonuclear leucocyte locomotion," *Semin. Cell Biol.*, vol. 1, pp. 125-34, 1990.
- [20] SH Zigmond, HI Levitsky, and BJ Kreel, "Cell polarity: An examination of its behavioral expression and its consequences for polymorphonuclear leukocyte chemotaxis," *J Cell Biol*, vol. 89, pp. 585-592, 1981.
- [21] Z Xiao, N Zhang, DB Murphy, and PN Devreotes, "Dynamic distribution of chemoattractant receptors in living cells during chemotaxis and persistent stimulation," *J Cell Biol*, vol. 139, pp. 365-374, 1997.
- [22] G Servant, OD Weiner, ER Neptune, JW Sedat, and HR Bourne, "Dynamics of a chemoattractant receptor in living neutrophils during chemotaxis," *Mol Biol Cell*, vol. 10, pp. 1163-78, 1999.
- [23] T Jin, M Amzel, PN Devreotes, and L Wu, "Selection of gbeta subunits with point mutations that fail to activate specific signaling pathways in vivo: dissecting cellular responses mediated by a heterotrimeric G protein in Dictyostelium discoideum," *Mol Biol Cell*, vol. 9, pp. 2949-2961, 1998.
- [24] M Ueda, Y Sako, T Tanaka, P Devreotes, and T Yanagida, "Single-molecule analysis of chemotactic signaling in Dictyostelium cells," *Science*, vol. 294, pp. 864-867, 2001.
- [25] C Janetopoulos, T Jin, and P Devreotes, "Receptor-mediated activation of heterotrimeric G-proteins in living cells," *Science*, vol. 291, pp. 2408-2411, 2001.
- [26] P Devreotes and C Janetopoulos, "Eukaryotic chemotaxis: distinctions between directional sensing and polarization," *J Biol Chem*, vol. 278, pp. 20445-8, 2003.
- [27] HG Othmer and P Schaap, "Oscillatory cAMP Signaling in the development of *Dictyostelium discoideum*," *Comments on Theoretical Biology*, vol. 5, pp. 175-282, 1998.
- [28] M Postma, J Roelofs, J Goedhart, TWJ Gadella, AJWG Visser, and PJM Van Haastert, "Uniform cAMP Stimulation of Dictyostelium Cells Induces Localized Patches of Signal Transduction and Pseudopodia," *Mol Biol Cell*, vol. 14, pp. 5019-5027, 2003.
- [29] SH Zigmond and SJ Sullivan, "Sensory Adaptation of Leukocytes to Chemotactic Peptides," *J Cell Biol*, vol. 82, pp. 517-527, 1979.
- [30] F Wang, P Herzmark, OD Weiner, S Srinivasan, G Servant, and HR Bourne, "Lipid products of PI(3)Ks maintain persistent cell polarity and directed motility in neutrophils," *Nat Cell Biol*, vol. 4, pp. 513-518, 2002.
- [31] A Gierer and H Meinhardt, "Theory of Biological Pattern Formation," *Kybernetik*, vol. 12, pp. 30-39, 1972.
- [32] AM Turing, "The Chemical Basis of Morphogenesis," *Philos Trans R Soc Lond B Biol Sci*, vol. 237, pp. 37-72, 1952.

- [33] H Meinhardt, "Orientation of chemotactic cells and growth cones: models and mechanisms," *J Cell Sci*, vol. 112, pp. 2867-2874, 1999.
- [34] A Narang, KK Subramanian, and DA Lauffenburger, "A mathematical model for chemoattractant gradient sensing based on receptor-regulated membrane phospholipid signaling dynamics," *Ann Biomed Eng*, vol. 29, pp. 677-91, 2001.
- [35] M Postma and PJ Van Haastert, "A diffusion-translocation model for gradient sensing by chemotactic cells," *Biophys J*, vol. 81, pp. 1314-1323, 2001.
- [36] A Levchenko and PA Iglesias, "Models of eukaryotic gradient sensing: application to chemotaxis of amoebae and neutrophils," *Biophys J*, vol. 82, pp. 50-63, 2002.
- [37] J Krishnan and PA Iglesias, "Analysis of the Signal Transduction Properties of a Module of Spatial Sensing in Eukaryotic Chemotaxis," *Bull Math Biol*, vol. 65, pp. 95-128, 2003.
- [38] W-J Rappel, PJ Thomas, H Levine, and WF Loomis, "Establishing direction during chemotaxis in eukaryotic cells," *Biophys J*, vol. 83, pp. 1361-1367, 2002.
- [39] KK Subramanian and A Narang, "A mechanistic model for eukaryotic gradient sensing: spontaneous and induced phosphoinositide polarization," *J Theor Biol*, vol. 231, pp. 49-67, 2004.
- [40] JM Haugh and IC Schneider, "Spatial Analysis of 3' Phosphoinositide Signaling in Living Fibroblasts: I. Uniform Stimulation Model and Bounds on Dimensionless Groups," *Biophys J*, vol. 86, pp. 589-598, 2004.
- [41] IC Schneider and JM Haugh, "Spatial Analysis of 3' Phosphoinositide Signaling in Living Fibroblasts: II. Parameter Estimates for Individual Cells from Experiments," *Biophys J*, vol. 86, pp. 599-608, 2004.
- [42] LR Stephens, A Eguinoa, H ErdjumentBromage, M Lui, F Cooke, J Coadwell, AS Smrcka, M Thelen, K Cadwallader, P Tempst, and PT Hawkins, "The G beta gamma sensitivity of a PI3K is dependent upon a tightly associated adaptor, p101," *Cell*, vol. 89, pp. 105-114, 1997.
- [43] HCE Welch, WJ Coadwell, CD Ellson, GJ Ferguson, SR Andrews, H Erdjument-Bromage, P Tempst, PT Hawkins, and LR Stephens, "P-Rex1, a PtdIns(3,4,5)P3- and G[beta][gamma]-Regulated Guanine-Nucleotide Exchange Factor for Rac," *Cell*, vol. 108, pp. 809-821, 2002.
- [44] OD Weiner, "Rac Activation: P-Rex1 -- A Convergence Point for PIP3 and G[beta][gamma]?", *Curr Biol*, vol. 12, pp. R429-R431, 2002.
- [45] HCE Welch, WJ Coadwell, LR Stephens, and PT Hawkins, "Phosphoinositide 3-kinase-dependent activation of Rac," *FEBS Lett*, vol. 546, pp. 93-97, 2003.
- [46] GM Bokoch, CJ Vlahos, Y Wang, UG Knaus, and AE Traynor-Kaplan, "Rac GTPase interacts specifically with phosphatidylinositol 3-kinase," *Biochem J*, vol. 315 ( Pt 3), pp. 775-9, 1996.
- [47] KF Tolias, JH Hartwig, H Ishihara, Y Shibasaki, LC Cantley, and CL Carpenter, "Type I alpha phosphatidylinositol-4-phosphate 5-kinase mediates Rac-dependent actin assembly," *Curr Biol*, vol. 10, pp. 153-156, 2000.
- [48] OD Weiner, PO Neilsen, GD Prestwich, MW Kirschner, LC Cantley, and HR Bourne, "A PtdInsP(3)- and Rho GTPase-mediated positive feedback loop regulates neutrophil polarity," *Nat Cell Biol*, vol. 4, pp. 509-13, 2002.

- [49] S Srinivasan, F Wang, S Glavas, A Ott, F Hofmann, K Aktories, D Kalman, and HR Bourne, "Rac and Cdc42 play distinct roles in regulating PI(3,4,5)P<sub>3</sub> and polarity during neutrophil chemotaxis," *J Cell Biol*, vol. 160, pp. 375-385, 2003.
- [50] H Ishihara, Y Shibasaki, N Kizuki, T Wada, Y Yazaki, T Asano, and Y Oka, "Type I phosphatidylinositol-4-phosphate 5-kinases. Cloning of the third isoform and deletion/substitution analysis of members of this novel lipid kinase family," *J Biol Chem*, vol. 273, pp. 8741-8748, 1998.
- [51] GB Willars, SR Nahorski, and RAJ Challiss, "Differential regulation of muscarinic acetylcholine receptor-sensitive polyphosphoinositide pools and consequences for signaling in human neuroblastoma cells," *J Biol Chem*, vol. 273, pp. 5037-5046, 1998.
- [52] S Cockcroft, "Mammalian phosphatidylinositol transfer proteins: emerging roles in signal transduction and vesicular traffic," *Chem Phys Lipids*, vol. 98, pp. 23-33, 1999.
- [53] MJ Berridge and RF Irvine, "Inositol phosphates and cell signalling," *Nature*, vol. 341, pp. 197-205, 1989.
- [54] EG Tall, I Spector, SN Pentyla, I Bitter, and MJ Rebecchi, "Dynamics of phosphatidylinositol 4,5-bisphosphate in actin-rich structures," *Curr Biol*, vol. 10, pp. 743-746, 2000.
- [55] A Honda, M Nogami, T Yokozeki, M Yamazaki, H Nakamura, H Watanabe, K Kawamoto, K Nakayama, AJ Morris, MA Frohman, and Y Kanaho, "Phosphatidylinositol 4-Phosphate 5-Kinase [alpha] Is a Downstream Effector of the Small G Protein ARF6 in Membrane Ruffle Formation," *Cell*, vol. 99, pp. 521-532, 1999.
- [56] SA Watt, G Kular, IN Fleming, CP Downes, and JM Lucocq, "Subcellular localization of phosphatidylinositol 4,5-bisphosphate using the pleckstrin homology domain of phospholipase C [Delta]1," *Biochem J*, vol. 363, pp. 657-666, 2002.
- [57] S Funamoto, R Meili, S Lee, L Parry, and RA Firtel, "Spatial and Temporal Regulation of 3-Phosphoinositides by PI 3-Kinase and PTEN Mediates Chemotaxis," *Cell*, vol. 109, pp. 611-623, 2002.
- [58] RL Doughman, AJ Firestone, ML Wojtasiak, MW Bunce, and RA Anderson, "Membrane ruffling requires coordination between type I phosphatidylinositol phosphate kinase and Rac signaling," *J Biol Chem*, vol. 278, pp. 23036-23045, 2003.
- [59] SH Zigmond, "How WASP regulates actin polymerization," *J Cell Biol*, vol. 150, pp. F117-F119, 2000.
- [60] TD Pollard, L Blanchoin, and RD Mullins, "Molecular mechanisms controlling actin filament dynamics in nonmuscle cells," *Annu Rev Biophys Biomol Struct*, vol. 29, pp. 545-576, 2000.
- [61] GG Borisov and TM Svitkina, "Actin machinery: pushing the envelope," *Curr Opin Cell Biol*, vol. 12, pp. 104-112, 2000.
- [62] YE Huang, M Iijima, CA Parent, S Funamoto, RA Firtel, and P Devreotes, "Receptor-mediated regulation of PI3Ks confines PI(3,4,5)P<sub>3</sub> to the leading edge of chemotaxing cells," *Mol Biol Cell*, vol. 14, pp. 1913-1922, 2003.

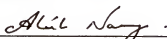
- [63] Numerical Algorithms Group, "NAG FORTRAN library introductory guide," Mark 18 ed. Oxford, UK, 1999.
- [64] TL Hill, *An introduction to statistical thermodynamics*, 1st ed. New York: Dover Publications, 1986.
- [65] DA Lauffenburger and JJ Linderman, *Receptors : Models for binding, trafficking, and signalling*. New York: Oxford University Press, 1993.
- [66] JM Shields and WS Haston, "Behaviour of neutrophil leucocytes in uniform concentrations of chemotactic factors: Contraction waves, cell polarity and persistence," *J Cell Sci*, vol. 74, pp. 75-93, 1985.
- [67] BS Kerner and VV Osipov, *Autosolitons: A new approach to problems of self organization and turbulence*, 1st ed. Dordrecht: Kluwer Academic Publishers, 1994.
- [68] PC Fife, *Mathematical aspects of reacting and diffusing systems*, vol. 28, 1st ed. Berlin: Springer-Verlag, 1979.
- [69] JA Murdock, *Perturbations : Theory and Methods*. New York: Wiley, 1991.
- [70] ED Conway, "Diffusion and predator-prey interaction: pattern in closed systems," in *Partial Differential Equations and Dynamical Systems (Research Notes in Mathematics)*, W. E. Fitzgibbon, Ed.: Pitman Advanced Pub. Program, 1984, pp. 83-133.
- [71] P Grindrod, *The theory and applications of reaction-diffusion systems*, 2nd ed. Oxford: Clarendon Press, 1996.
- [72] AB Hauert, S Martinelli, C Marone, and V Niggli, "Differentiated HL-60 cells are a valid model system for the analysis of human neutrophil migration and chemotaxis," *Int J Biochem Cell Biol*, vol. 34, pp. 838-54, 2002.
- [73] C Brock, M Schaefer, HP Reusch, C Czupalla, M Michalke, K Spicher, G Schultz, and B Nurnberg, "Roles of G beta gamma in membrane recruitment and activation of p110 gamma/p101 phosphoinositide 3-kinase gamma," *J Cell Biol*, vol. 160, pp. 89-99, 2003.
- [74] OD Weiner, "Rac activation: P-Rex1 - a convergence point for PIP(3) and Gbetagamma?," *Curr Biol*, vol. 12, pp. R429-31, 2002.
- [75] C Sadhu, B Masinovsky, K Dick, CG Sowell, and DE Staunton, "Essential role of phosphoinositide 3-kinase delta in neutrophil directional movement," *J Immunol*, vol. 170, pp. 2647-54, 2003.
- [76] KF Tolia, LC Cantley, and CL Carpenter, "Rho-Family Gtpases Bind to Phosphoinositide Kinases," *J Biol Chem*, vol. 270, pp. 17656-17659, 1995.
- [77] PB van Hennik, JP ten Klooster, JR Halstead, C Voermans, EC Anthony, N Divecha, and PL Hordijk, "The C-terminal domain of Rac1 contains two motifs that control targeting and signaling specificity," *J Biol Chem*, vol. 278, pp. 39166-39175, 2003.
- [78] PAO Weernink, K Meletiadis, S Hommeltenberg, M Hinz, H Ishihara, M Schmidt, and KH Jakobs, "Activation of type I phosphatidylinositol 4-phosphate 5-kinase isoforms by the Rho GTPases, RhoA, Rac1, and Cdc42," *J Biol Chem*, vol. 279, pp. 7840-7849, 2004.

- [79] M Hannigan, L Zhan, Z Li, Y Ai, D Wu, and CK Huang, "Neutrophils lacking phosphoinositide 3-kinase gamma show loss of directionality during N-formyl-Met-Leu-Phe-induced chemotaxis," *Proc Natl Acad Sci U S A*, vol. 99, pp. 3603-8, 2002.
- [80] EM Gardiner, KN Pestonjamas, BP Bohl, C Chamberlain, KM Hahn, and GM Bokoch, "Spatial and temporal analysis of Rac activation during live neutrophil chemotaxis," *Curr Biol*, vol. 12, pp. 2029-34, 2002.
- [81] NEH Chatah and CS Abrams, "G-protein-coupled receptor activation induces the membrane translocation and activation of phosphatidylinositol-4-phosphate 5-kinase I alpha by a Rac- and Rho-dependent pathway," *J Biol Chem*, vol. 276, pp. 34059-34065, 2001.
- [82] OD Weiner, G Servant, MD Welch, TJ Mitchison, JW Sedat, and HR Bourne, "Spatial control of actin polymerization during neutrophil chemotaxis," *Nat Cell Biol*, vol. 1, pp. 75-81, 1999.
- [83] RL Doughman, AJ Firestone, and RA Anderson, "Phosphatidylinositol phosphate kinases put PI4,5P(2) in its place," *J Membr Biol*, vol. 194, pp. 77-89, 2003.
- [84] MG Coppolino, R Dierckman, J Loijens, RF Collins, M Pouladi, J Jongstra-Bilen, AD Schreiber, WS Trimble, R Anderson, and S Grinstein, "Inhibition of phosphatidylinositol-4-phosphate 5-kinase Ialpha impairs localized actin remodeling and suppresses phagocytosis," *J Biol Chem*, vol. 277, pp. 43849-57, 2002.
- [85] EL de Hostos, B Bradtke, F Lottspeich, R Guggenheim, and G Gerisch, "Coronin, an actin binding protein of Dictyostelium discoideum localized to cell surface projections, has sequence similarities to G protein beta subunits," *EMBO J.*, vol. 10, pp. 4097-104, 1991.
- [86] ME Monaco and JR Adelson, "Evidence for Coupling of Resynthesis to Hydrolysis in the Phosphoinositide Cycle," *Biochem J*, vol. 279, pp. 337-341, 1991.
- [87] B Alberts, *Molecular biology of the cell*, 3rd ed. New York: Garland, 1994.


## BIOGRAPHICAL SKETCH

Kulandayan Kasi Subramanian was born on March 25, 1978, to Seetha Subramanian and Subramanian Kasi in Chennai, Tamil Nadu, India. He graduated from Padma Seshadri Senior Secondary School, Chennai, India, in 1995. Kulandayan entered the Bachelor of Technology program in chemical engineering at Sri Venkateshwara College of Engineering, University of Madras, Pennalur, India, in 1995 and graduated with honors in 1999. In August 1999, Kulandayan entered the master's program at Department of Chemical Engineering, College of Engineering, University of Florida. He then transferred to the Ph.D. program in chemical engineering in August 2000, and worked under the guidance of Dr. Atul Narang. Kulandayan received his Doctor of Philosophy degree in engineering in December 2004.


I certify that I have read this study and that in my opinion it conforms to acceptable standards of scholarly presentation and is fully adequate, in scope and quality, as a dissertation for the degree of Doctor of Philosophy.

  
Atul Narang, Chairman  
Assistant Professor of Chemical Engineering

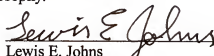
I certify that I have read this study and that in my opinion it conforms to acceptable standards of scholarly presentation and is fully adequate, in scope and quality, as a dissertation for the degree of Doctor of Philosophy.

  
Gerard Patrick James Shaw, Cochairman  
Professor of Neuroscience


I certify that I have read this study and that in my opinion it conforms to acceptable standards of scholarly presentation and is fully adequate, in scope and quality, as a dissertation for the degree of Doctor of Philosophy.

  
Ranga Narayanan  
Professor of Chemical Engineering

I certify that I have read this study and that in my opinion it conforms to acceptable standards of scholarly presentation and is fully adequate, in scope and quality, as a dissertation for the degree of Doctor of Philosophy.

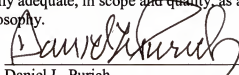
  
Lewis E. Johns  
Professor of Chemical Engineering

I certify that I have read this study and that in my opinion it conforms to acceptable standards of scholarly presentation and is fully adequate, in scope and quality, as a dissertation for the degree of Doctor of Philosophy.

  
Richard B. Dickinson  
Associate Professor of Chemical Engineering



I certify that I have read this study and that in my opinion it conforms to acceptable standards of scholarly presentation and is fully adequate, in scope and quality, as a dissertation for the degree of Doctor of Philosophy.



---

Daniel L. Purich  
Professor of Biochemistry and Molecular  
Biology

This dissertation was submitted to the Graduate Faculty of the College of Engineering and to the Graduate School and was accepted as partial fulfillment of the requirements for the degree of Doctor of Philosophy.

December 2004



---

Pramod P. Khargonekar  
Dean, College of Engineering

---

Kenneth Gerhardt  
Interim Dean, Graduate School